**Title:** Alternate splice variants of the mitochondrial fission protein *DNM1L*/Drp1 regulate mitochondrial dynamics and cell fate in ovarian cancer.

**Authors:** Zaineb Javed[1,2], Dong Hui Shin[2,β], Weihua Pan[1], Sierra R. White[1], Yeon Soo Kim[2,χ], Amal Taher Elhaw[1,2], Shriya Kamlapurkar[1], Ya-Yun Cheng[1], J Cory Benson[3], Ahmed Emam Abdelnaby[3], Rebecca Phaeton[4,δ], Hong-Gang Wang[5], Shengyu Yang[6], Mara L.G. Sullivan[7], Simon C. Watkins[7], Steven J. Mullett[3, 8], Stacy L. Gelhaus[3, 8], Nam Lee[9], Lan G. Coffman[1], Katherine M. Aird[3], Mohamed Trebak[3,10], Karthikeyan Mythreye[11], Vonn Walter[12], Nadine Hempel[1,α]

[1] Department of Medicine, Division of Hematology/Oncology, UPMC Hillman Cancer Center, University of Pittsburgh School of Medicine, PA, USA

[2] Department of Pharmacology, College of Medicine, Pennsylvania State University, Hershey, PA, USA

[3] Department of Pharmacology and Chemical Biology, University of Pittsburgh School of Medicine, PA, USA

[4] Department of Obstetrics & Gynecology, College of Medicine, Pennsylvania State University, Hershey, PA, USA

[5] Department of Pediatrics, College of Medicine, Pennsylvania State University, Hershey, PA, USA

[6] Department of Cellular and Molecular Physiology, College of Medicine, Pennsylvania State University, Hershey, PA, USA

[7] Center for Molecular Imaging, University of Pittsburgh School of Medicine, PA, USA

[8] Health Sciences Mass Spectrometry Core, University of Pittsburgh, PA, USA

[9] Division of Pharmacology, Chemistry and Biochemistry, College of Medicine, University of Arizona, Tucson, AZ, USA

[10] Vascular Medicine Institute (VMI), University of Pittsburgh School of Medicine, PA, USA

28 [11] Department of Pathology and O'Neal Comprehensive Cancer Center, Heersink School of
29 Medicine, University of Alabama at Birmingham, Birmingham, AL, USA

30 [12] Department of Public Health Sciences, Division of Biostatistics and Bioinformatics and
31 Department of Biochemistry and Molecular Biology, College of Medicine, Pennsylvania State
32 University, Hershey, PA, USA

33

34

35 **[α]Corresponding Author:**
36 University of Pittsburgh School of Medicine, Division of Hematology/Oncology
37 UPMC Hillman Cancer Center
38 The Assembly, Rm 2039
39 5051 Centre Ave, Pittsburgh, PA 15213
40 Ph: 412-648-4822
41 nah158@pitt.edu
42
43
44 Current Address:
45 [β] School of Pharmacy, Virginia Commonwealth University, Richmond, VA, USA
46 [χ] Division of Human Biology, Fred Hutchinson Cancer Center, Seattle, WA, USA
47 [δ] GlaxoSmithKline, Collegeville, PA, USA

## Abstract

Aberrant mitochondrial fission/fusion dynamics have previously been reported in cancer cells. While post translational modifications are known regulators of GTPases of the mitochondrial fission/fusion machinery, we show for the first time that alternate splice variants of the fission protein Drp1 (*DNM1L*) have specific and unique roles in ovarian cancer, adding to the complexity of mitochondrial fission/fusion regulation in tumor cells. We find that ovarian cancer specimens express a Drp1 alternate splice transcript variant lacking exon 16 of the variable domain. High expression of Drp1 lacking exon 16 relative to other transcripts is associated with poor patient outcome. Unlike the full length variant, expression of Drp1 lacking exon 16 leads to decreased association of Drp1 to mitochondrial fission sites, more fused mitochondrial networks, enhanced respiration and TCA cycle metabolites, and is associated with a more tumorigenic phenotype. These effects can also be reversed by specific siRNA-mediated inhibition of the endogenously expressed transcript lacking exon 16. Moreover, lack of exon 16 abrogates mitochondrial fission in response to pro-apoptotic stimuli and leads to decreased sensitivity to chemotherapeutics. These data emphasize the significance of the pathophysiological consequences of Drp1 alternate splicing and divergent functions of Drp1 splice variants, and strongly warrant consideration of Drp1 splicing in future studies.

## Introduction

Mitochondria are highly dynamic organelles continuously undergoing fission and fusion events to facilitate adaptations to cellular and extracellular cues. The opposing processes of mitochondrial fission and fusion are mediated by several evolutionarily conserved dynamin-related GTPases, including Mitofusins (Mfn1&2) and Opa1 which promote fusion and Dynamin-related Protein 1 (Drp1) which mediates mitochondrial fission [1, 2]. Drp1, which is encoded by the gene *DNM1L*, forms homo-multimeric helical structures around the outer mitochondrial membrane to initiate division, and is tightly regulated by post-translational modifications, oligomerization and interaction with proteins that anchor Drp1 to mitochondria [3-7]. Given that the shape of mitochondria are inextricably linked to their function, maintaining a balance between these dynamic fission and fusion events is essential in preserving mitochondrial respiration, and for the proper distribution of mitochondria and mitochondrial DNA during mitosis [8, 9]. Moreover, mitochondrial fission is also an integral component of the apoptotic and mito/autophagy pathways [10, 11]. Perturbation in mitochondrial fission/fusion dynamics have been implicated in cancer, and cancer cells can exploit adaptive mitochondrial dynamics to their advantage for meeting their heightened energy demands and to regulate cellular processes including tumor metabolism, stress response pathways and resistance to apoptosis. Several studies have described a role for enhanced fission in cancer [12-14], and this shown to be associated with cell cycle progression [15, 16] and migration [17]. Underlying genetic factors may also contribute to exacerbated signaling that drives the activation of fission, as observed in BRAF and KRAS mutant tumors where Drp1 phosphorylation of S616 is activated via Erk [13, 14, 18]. On the contrary, mitochondrial fission is associated with apoptosis and decreased fission can result in apoptosis resistance [11, 19-21]. Enhanced fusion may thus be one mechanism by which tumors evade apoptosis in response to chemotherapeutic agents [22, 23]. These seemingly conflicting studies appear to suggest that both aberrant fission and fusion could have important roles during tumor progression and that the dysregulation of mitochondrial fission and fusion dynamics has the potential to influence various aspects of cancer, including progression, recurrence, and chemoresistance.

In addition to regulation by post-translational mechanisms, alternative splicing of the *DNM1L* pre-mRNA transcript has been shown to give rise to Drp1 splice variants with differential tissue expression, subcellular localization and fission activity [24-29]. However, despite the established importance of Drp1 as an integral mitochondrial fission protein few studies have investigated the expression and unique functions of Drp1 splice variants in pathophysiological contexts. The current study builds on our observations that ovarian cancer cell lines display

99 heterogeneous mitochondrial fission along with corresponding variations in Drp1 protein
100 expression [30]. While Drp1 has been shown to be overexpressed in several tumor types, the role
101 of individual splice variants was not considered in these studies. In ovarian cancer *DNM1L* gene
102 amplification has been associated with poor patient outcomes [12, 31]. However, it is unclear how
103 this reflects the relative expression and function of Drp1 splice variants. Here, we show for the
104 first time that transcripts arising from exon 16 splicing are highly expressed in ovarian cancer
105 cells and that relative expression of this transcript to full length Drp1 mRNA is predictive of poor
106 patient outcome. Relative to the most studied Drp1 transcript that includes all exons, we
107 demonstrate that exon 16 splicing results in a Drp1 protein with a unique function related to
108 regulation of mitochondrial architecture, mitochondrial function, tumor metabolism and
109 chemosensitivity in tumor cells. This represents the first study demonstrating the
110 pathophysiological relevance of Drp1 splice variants.
111

112 ## Results

113 **Ovarian cancer cells display distinct Drp1/*DNM1L* splice variant expression.**

114 We previously observed that ovarian cancer cell lines express several different
115 molecular weight protein variants of Drp1 [30]. To determine the clinical significance of this
116 observation, Drp1 protein expression was assessed in ascites-derived epithelial ovarian cancer
117 (EOC) cells from ovarian cancer patients (Fig. 1a). Four bands ranging in molecular weight
118 between ~75- 85kDa were detected, with two being more prominently expressed, and the
119 propensity for the lower molecular weight band of these to be present in samples of high grade
120 serous ovarian adenocarcinoma (HGSA: ECO7, EOC14, EOC15 (Fig. 1a). Similarly, two major
121 Drp1 protein bands were also observed in OVCA420 and OVCA433 ovarian cancer cells lines
122 and these validated as being Drp1 using siRNA mediated knock down (Fig. 1b). Several
123 Drp1/*DNM1L* transcript variants are annotated on the RefSeq record, including alternate splicing
124 of exons 3, 16 and 17 [7, 27, 28, 32, 33]. To determine if the observed Drp1 protein variants are due to
125 alternate start site utilization, splicing or alternate transcriptional termination, 5' and 3' rapid
126 amplification of cDNA ends (RACE) was carried out. 3'RACE revealed that ovarian cancer cells
127 express multiple Drp1 transcripts, including alternate splicing of exons 16 and 17, differential
128 3'UTR lengths, and identification of short transcripts that terminate after exon 14 (ΔC-Ex14) and
129 in intron 17 (ΔC-In17) at predicted alternate polyadenylation sites (Fig. 1c, d and Extended Data
130 Fig. 1a, c). 5'RACE demonstrated utilization of the same transcriptional start site and a lack of
131 exon 3 for all transcripts (Extended Data Fig. 1b, c). The ΔC-In17 transcript displayed alternate
132 splicing of exon 16 and had a predicted alternate stop codon within intron 17, leading to a

133 transcript with a novel coding sequence for 16 amino acids derived from intron 17 (Extended
134 Data Fig. 1c, d). It is predicted to express a 65 kDa protein lacking the C-terminal GED domain
135 (Fig. 1d, e), and using a polyclonal antibody, we were able to detect a protein at the predicted
136 size which was decreased in expression following siRNA mediate Drp1 knock-down (Extended
137 Data Fig. 1g). This could not be detected when using a monoclonal antibody targeting the C-
138 terminus (Fig. 1b and Extended Data Fig. 1f), suggesting that the ΔC-In17 transcript may result
139 in expression of a truncated protein. ΔC-In17 was detected to variable degrees in other ovarian
140 cancer cell lines and patient derived tumor cells by RT-PCR (Extended Data Fig. 1e, and
141 Extended Data Fig. 3a). While the functional consequences of this novel C-terminal truncation
142 transcript require further study, annotation of TCGA ovarian cancer data for the ΔC-In17
143 transcripts demonstrated that these were only detected in <15% of TCGA ovarian cancer
144 specimens (Fig. 2a). Thus, we focused on alternate splice variants of the variable domain exons
145 16 and 17 in full length Drp1, as these are predicted to yield proteins of molecular weights
146 between 78-82kDa, matching the major protein variants observed in patient ascites derived
147 EOCs (Fig. 1a, b). Exons 16 and 17 are located in the variable B-domain of Drp1 (Fig. 1e) and
148 alternate splicing of these exons was further examined using RT-PCR with primers flanking the
149 variable domain. Variable expression of splice variants was found in a panel of ovarian cancer
150 cell lines (Fig. 1f), with the HGSA cell lines OVCAR3, OVCA420 and OVCA433 demonstrating a
151 higher relative expression of the transcript with exon 16 spliced out, referred here after as
152 Drp1(-/17).
153
154 **Patient ascites derived epithelial ovarian cancer cells and tumor specimens display high**
155 **expression of Drp1 transcript variants lacking exon 16, which is associated with poor**
156 **patient outcome.**
157 By annotating TCGA RNA sequencing data for the identified Drp1/*DNM1L* transcript
158 variants we found that all variable domain (Exons 16 and 17) splice variants of the full-length
159 transcripts were expressed to varying degrees in TCGA specimens (Fig. 2a, b). Of the four
160 variable domain variants, highest levels of Drp1(-/17), the transcript lacking exon 16, was
161 observed, followed by Drp1(16/17) and Drp1(-/-) displaying approximately equal expression
162 (Fig. 2b). Drp1(16/-), the transcript lacking exon 17, was least abundant. Similar to our findings
163 in cell lines, most Drp1/*DNM1L* transcripts in TCGA specimens lacked exon 3 (Extended Data
164 Fig. 2a), agreeing with previous work describing exon 3 retention to be predominant in neuronal
165 tissues [27]. TCGA data were independently validated by assessing splice variant transcript
166 abundance in EOCs isolated from patient ascites (Fig. 2c) and in a separate cohort of matched

normal fallopian and omental or ovarian tumor specimens (Fig. 2d). Ascites-derived EOCs classified as HGSA and carcinosarcoma demonstrated predominant expression of the splice variant lacking exon 16, Drp1(-/17), and transcripts containing both exons 16 and 17, Drp1(16/17). The majority of matched samples displayed an increase in relative Drp1(-/17) expression in ovarian tumors (11/13 specimens) and omental tumors (5/5) compared to benign/normal fallopian tube (Fig. 2d; Extended Data Fig. 3). These data demonstrate that ovarian cancer cells express several Drp1/*DNM1L* splice variants, with a high abundance of Drp1(-/17) expression, suggesting that splicing of exon 16 and retention of exon 17 might be of significance to ovarian cancer.

We were curious if predominance of Drp1 splice variant expression is predictive of patient outcome. While patients with high expression of Drp1(-/17) trended towards worse overall survival (Fig. 2e), comparisons between high and low expression of individual Drp1 splice variants was not able to significantly predict survival (Extended Data Fig. 2b). However, grouping patients into mutually exclusive high vs low expression of splice variant pairs based on median expression cut-offs, revealed that relative abundance of the different variable domain splice variants influenced patient outcome (Fig. 2f; Extended Data Fig. 2c, d). Patients with tumors displaying high Drp1(-/17) and low Drp1(16/17) expression demonstrated poor overall survival compared to those with high Drp1(16/17) and low Drp1(-/17) expression (HR: 1.81, 95% CI: 1.076 to 3.071, log rank p=0.0208), with a median survival difference of 14.3 months (Fig. 2f). High Drp1(-/17):low Drp1(16/-) expression also decreased median survival by 11.7 months, albeit not significantly (HR: 1.508, 95% CI: 0.9304 to 2.444, log rank p=0.088), and other mutually exclusive expression comparisons between Drp1 splice variants were not significantly predictive of survival (Extended Data Fig. 2d). Although Drp1(16/17) and Drp1(-/17) transcript variants are both abundant in ovarian cancer cell lines and patient specimens, the above data suggest that their relative expression has consequences on ovarian cancer progression. Yet, the significance of exon 16 splicing on Drp1 function in cancer cells remains unexplored.

**Loss of Exon 16 abrogates association with mitochondrial fission puncta and leads to more fused mitochondrial networks.**

The HGSA OVCA433 cell lines was chosen as a model for subsequent studies as it displayed similar *DNM1L* variable domain transcript expression as HGSA patient specimens, while SKOV3 cells were chosen as a model due to their relatively equal expression of all four full length variable domain variants. To investigate their function, Drp1 splice variants were

201 expressed as GFP fusion proteins by lentiviral transduction in both cell lines (Fig. 3a and
202 Extended Data Fig. 4a). Drp1(16/17) which contains exons 16 and 17 was localized in both the
203 cytosol and at distinct mitochondrial fission puncta, as previously described by numerous Drp1
204 overexpression studies [6, 27, 34]. On the contrary, Drp1(-/17) co-localized less with mitochondria,
205 with fewer distinct fission puncta observed. Instead, Drp1(-/17) displayed a filamentous pattern
206 of localization (Fig. 3b). Consistent with the work by Strack and Cribbs, who demonstrated that
207 the splicing of exon 16 modifies the association of Drp1 with mitochondria and increases binding
208 to microtubules [27], we found that Drp1(-/17) exhibited co-localization with tubulin in ovarian
209 cancer cells (Fig. 3b,c and extended Data Fig. 4b,c).
210 The expression of Drp1(-/17) was previously reported to lead to more fused and
211 elongated mitochondrial network, likely due to the reduced association of Drp1(-/17) with
212 mitochondria [27]. In line with this, compared to both GFP control and Drp1(16/17), cells
213 expressing Drp1(-/17) had longer average mitochondrial branch lengths and a greater number
214 of branches per mitochondria, indicative of a more interconnected mitochondrial network (Fig.
215 3d, and extended data Fig. 4d). In contrast, expression of Drp1(16/17) led to shorter branch
216 lengths and fewer branches per mitochondria, a predicted phenotype following overexpression
217 of Drp1 (Fig. 3d, Extended Data 4&5). TEM imaging additionally demonstrated elongated
218 mitochondrial phenotypes in Drp1(-/17) expressing cells, contrasting with the smaller, more
219 circular mitochondria seen following expression of Drp1(16/17) (Fig. 3e, f and Extended Data
220 Fig. 4e and 5). Notably, expression of Drp1(-/17) led to an overall higher number and density of
221 cristae per mitochondria (Fig. 3e, f and Extended Data Fig. 5).
222 After exposure to the pro-fission stimulus FCCP cells expressing Drp1(-/17) did not
223 increase the number of Drp1 containing fission puncta as seen with expression of Drp1(16/17).
224 Instead, Drp1(-/17) continued to exhibit high association with the microtubule network and
225 mitochondria maintained their elongated mitochondrial morphology (Extended Data Fig. 6).
226 These observations suggest that high expression of Drp1(-/17) could lead to abrogated
227 mitochondrial fission and a more fused mitochondrial network, likely because of its lower
228 association with mitochondrial fission puncta and partial localization to microtubules, and that
229 cells expressing Drp1(-/17) have reduced response to pro-fission stimuli. These findings are
230 significant, as Drp1(-/17) is highly expressed in tumor cells, yet past studies have primarily
231 investigated the function of Drp1 in cancer cells by overexpressing the Drp1(16/17) variant
232 transcript that includes both exons 16 and 17. Thus, we next investigated the functional
233 consequences of Drp1(-/17) expression in ovarian cancer cells.
234

235 **Expression of Drp1(-/17) increases oxygen consumption and alters tumor cell**
236 **metabolism.**

237 Due to their continuous membranes and matrix lumens, fused mitochondrial networks
238 can facilitate better diffusion of molecules, including ADP, and reducing equivalents NADH and
239 FADH2, necessary for oxidative phosphorylation [35, 36]. In addition, a more ordered cristae
240 architecture improves electron transport chain super complex assembly, and these structural
241 features have been associated with optimal mitochondrial respiration [37-39]. Given that Drp1(-/17)
242 splice variant expression leads to enhanced mitochondrial networks and cristae numbers the
243 effects on mitochondrial respiration and cellular metabolism were assessed. Using extracellular
244 flux analysis significant increases in basal oxygen consumption rates (OCR), ATP-dependent
245 OCR and spare respiratory reserve were observed between Drp1(-/17) and Drp1(16/17)
246 expressing OVCA433 cells (Fig. 4a, b). An increase in OCR was similarly observed in SKOV3
247 cells expressing Drp1(-/17) (Extended Data Fig. 7). There were no differences in the expression
248 of mitochondrial proteins COX-I (complex IV), and SDH-A (Complex II) following expression of
249 either Drp1 variant suggesting that changes in mitochondrial activity are likely not attributable to
250 changes in mitochondrial biogenesis (Extended Data Fig. 8a, b). In addition, no consistent
251 changes in mitochondrial membrane potential or significant changes in mitoSox fluorescence,
252 an indicator of mitochondrial oxidant production, were associated with the expression of either
253 Drp1 variant in the cell lines tested (Extended Data Fig. 8c, d).
254 Compared to Drp1(16/17) or GFP controls, untargeted metabolomics (Fig. 4c) showed
255 that cells expressing Drp1(-/17) also display an increase in metabolites linked to glycolysis and
256 the pentose phosphate pathway. Related to the observed increases in lactate levels, an
257 increase in extracellular acidification rate was also seen, although this was not significant in
258 OVCA433 cells (Extended Data Fig. 7c-f). Select metabolites necessary for *de novo* purine and
259 pyrimidine synthesis, such ribulose-5-phosphate, glycine and aspartate, and most TCA cycle
260 metabolites were also elevated following overexpression of Drp1(-/17) relative to GFP control
261 and Drp1(16/17) (Fig. 4c). These changes were also accompanied by elevated total NAD(H)
262 levels and a decrease in the NAD+/NADH ratio (Fig. 4d and Extended Data Fig. 7g), which may
263 be contributing to the reducing equivalents for increased respiration seen in Drp1(-/17) cells.
264 Collectively, these findings suggest that enhanced Drp1(-/17) expression leads to an energetic
265 phenotype and alters metabolism of ovarian cancer cells compared to cells expressing
266 Drp1(16/17).

267

268 **Drp1(-/17) expression is advantageous to the tumorigenic properties of ovarian cancer**
269 **cells.**

270 *DNM1L* gene amplification has been reported to correlate with cell cycle gene
271 expression and poor patient outcomes in chemoresistant and recurrent ovarian cancer cases [12].
272 However, previous work did not account for expression of specific Drp1 splice variants, and it is
273 thus unknown which Drp1 transcript variant is specifically associated with proliferation and
274 chemoresistance. Considering that TCGA serous ovarian cancer patients with high Drp1(-/17)
275 expression relative to low Drp1(16/17) expression exhibited a lower median overall survival, we
276 further assessed the impact of Drp1 variable domain variant expression on tumor cell behavior.
277 Clonogenicity assays demonstrated that Drp1(-/17) expression maintained high clonogenic
278 potential similar to GFP controls, while expression of Drp1(16/17) was detrimental to single cell
279 survival (Fig. 5a). Importantly, only Drp1(-/17) expression significantly increased the proliferation
280 rate of both SKOV3 and OVCA433 (Fig. 5b). Cells expressing Drp1(-/17) notably also exhibited
281 a strong increase in migration compared to GFP and Drp1(16/17) expressing cells (Fig. 5c).
282 Taken together, these data show for the first time that expression of different Drp1 splice
283 variants influences tumor cell behavior and that high expression of Drp1(-/17) compared to
284 Drp1(16/17) is predominantly advantageous to ovarian cancer cells.
285

286 **Drp1(-/17) protects cells against chemotherapy induced apoptosis.**

287 Some studies have suggested that mitochondrial fission plays an integral part in the
288 initiation of apoptosis[11, 19, 40], and Drp1(-/17) expression was previously shown to prevent
289 staurosporin-mediated cell death[27]. We thus sought to test if high expression of Drp1(-/17) and
290 the concomitant increase in fused mitochondria may be beneficial to tumor cells when
291 challenged with cisplatin or paclitaxel treatment (Fig. 6a). Expression of Drp1(-/17) led to a
292 statistically significant increase in IC50 values for both compounds in OVCA433 and SKOV3
293 cells relative to GFP controls (Fig. 6b). Conversely, Drp1(16/17) expression enhanced cell death
294 in response to both compounds compared to GFP control cells, which was particularly evident
295 with Cisplatin (Fig. 6a, b). Notably, cells with Drp1(16/17) expression exhibited the highest
296 caspase 3/7 activity in response to both agents (Fig. 6c), while Drp1(-/17) expression
297 significantly abrogated caspase activity relative to GFP and Drp1(16/17) expressing cells in
298 response to cisplatin and paclitaxel. These data suggest that Drp1(16/17) mediated
299 mitochondrial fission enhances apoptosis of ovarian cancer cells, but that expression of Drp1(-
300 /17), which leads to abrogated mitochondrial fission, protects cells from apoptosis. To determine

301 if the differences in apoptosis initiation following expression of Drp1 splice variants is due to
302 their differential activation in response to chemotherapeutic agents, phosphorylation of Serine
303 616 was investigated. Basally, Drp1(-/17) protein displayed less Serine 616 phosphorylation
304 than Drp1(16/17) (Fig. 6d). Although predominantly observed in OVCA433 cells, Drp1(16/17)
305 was more susceptible to phosphorylation at S616 upon treatment with both cisplatin and
306 paclitaxel, while no change in phosphorylation was observed in Drp1(-/17) in response to these
307 agents (Fig. 6e). Taken together, these observations suggest that cells expressing Drp1(-/17)
308 might possess a survival advantage under the selective pressure exerted by chemotherapy, and
309 that this could be partially driven by abrogated phosphorylation in response to pro-apoptotic
310 stimuli.

311

312 **Endogenous manipulation of Drp1 splice variant expression validates the pro-**
313 **tumorigenic function of Drp1(-/17).**

314 The data above clearly demonstrate that overexpression of Drp1(-/17), the splice variant
315 lacking exon 16, has significantly different effects on mitochondrial morphology and function,
316 tumor cell behavior and chemosensitivity compared to expression of the full length Drp1(16/17).
317 To rule out that these observations are due to overexpression of recombinant protein, we
318 sought to assess whether altering the endogenous ratios of Drp1 splice variants could elicit
319 similar effects. To achieve this, splice variant-specific siRNAs targeting each of the four
320 endogenous variable domain Drp1/*DNM1L* splice variants were designed (Fig. 7a, b), and used
321 in SKOV3 cells as a model, as this cell line displayed relatively equal expression of all four
322 variable domain Drp1 transcript variants (Fig. 7a), thus allowing us to tune the ratios of their
323 relative expression using siRNAs. Specific knock-down of individual splice variants transcripts
324 (Fig. 7a) led to altered Drp1 protein variant expression (Fig. 7b). While it was more difficult to
325 resolve Drp1(16/17) and Drp1(16/-) on SDS-PAGE due to their close molecular weight
326 individual knockdowns of Drp1 protein variants could be distinctly visualized (Fig. 7b). A positive
327 control siRNA designed to target Exon 15 led to decreased protein expression of all variants
328 (Fig. 7b, lane 2). The knock-down of all variants (siDrp1 total) resulted in fused mitochondrial
329 morphology as expected, and as demonstrated by previous studies targeting Drp1 by RNAi [41-43]
330 (Fig. 7c,d). While knocking down each variant did enhance mitochondrial length and networking
331 to some extent, we observed a varying degree of impact depending on the specific variant
332 targeted (Fig. 7c, d and Extended Data Fig. 9a, b). Drp1(16/17) knockdown most closely
333 replicated the highly elongated mitochondrial morphology and increased branching seen with

334 total Drp1 knockdown (siDrp1-total, Fig. 7c, d). In contrast, the knockdown of siDrp1(-/17)
335 resulted in less substantial increases in mitochondrial length and networking (Fig. 7c, d), again
336 highlighting that Drp1(-/17) contributes less to mitochondrial fission than Drp1 (16/17).
337 Knockdowns of Drp1(-/16) and siDrp1(-/-) resulted in less elongated mitochondrial morphology
338 compared to siDrp1(16/17), albeit with slight increases compared to siDrp1(-/17) (Extended
339 Data Fig. 9a, b). The combination knockdown of Drp1(-/16) and Drp1(-/-), which essentially
340 enriches for higher but equal expression of Drp1(16/17) and Drp1(-/17), led to an intermediary
341 increase in mitochondrial length and branching (Fig. 7c, d). This suggests that the endogenous
342 ratio of expression between the Drp1(16/17) and Drp1(-/17) variants may be critical in
343 determining the overall fission activity of Drp1. Collectively, these results confirm our
344 overexpression data (Fig. 3), suggesting that the Drp1(16/17) variant plays a more active role in
345 Drp1-mediated mitochondrial fission, while Drp1(-/17) may have a lower capacity to elicit
346 mitochondrial fission.

347 Importantly, the functional consequences of altered Drp1 splice variants expression on
348 mitochondrial function could similarly be recapitulated using siRNA to target endogenous Drp1
349 transcripts. We previously showed that Drp1(16/17) overexpression was detrimental to
350 mitochondrial respiratory function while Drp1(-/17) overexpression improved OCR (Fig. 4 and
351 Extended Data Fig. 7). In concurrence, inhibition of Drp1(16/17) improved respiration while
352 siRNA targeting of Drp1(-/17) decreased both basal and ATP-linked oxygen consumption rate
353 (OCR) when compared to siRNA control transfected cells (Fig. 8a, b). No significant changes in
354 mitochondrial function were observed upon combined knockdown of Drp1(16/-) and Drp1(-/-),
355 which maintained equal expression of Drp1(16/17) and Drp1(-/17) (Fig. 8c), again suggesting
356 that an imbalance of their expression may lead to very different mitochondrial morphology and
357 functional consequences.

358 Subsequently, we investigated the changes in cellular proliferation and migration upon
359 perturbation of endogenous Drp1 variants (Fig. 8d, e, f). Compellingly, increased cellular
360 proliferation was only seen when Drp1(16/17) was knocked down, or when specific enrichment
361 of Drp1(-/17) was achieved by a combined knockdown of the other three variable domain
362 variants (siDrp1(16/17),(-/16) and (-/-); Fig. 8e). These conditions mimic Drp1(-/17)
363 overexpression (Fig. 5b) and mirror the low Drp1(16/17):high Drp1(-/17) expression observed in
364 the TCGA patient cohort that was marked by poor patient outcome (Fig. 2f). All other individual
365 or combination knock-downs of Drp1 transcript variants had little effect on proliferation (Fig. 8e
366 and Extended Data Fig. 9d). Moreover, cell migration was enhanced following single knockdown

367 of Drp1(16/17), whereas it significantly decreased after single knockdown of Drp1(-/17) variant
368 compared to the control (Fig. 8f). No difference in migration was observed in cells with equal
369 expression of Drp1(-/17) and Drp1(16/17) in following siDrp1(-/16) & Drp1(-/-) knock-down or in
370 cells with single knockdown of either Drp1(16/-) or Drp1(-/-) (Fig. 8f and Extended Data Fig. 9d).
371 Finally, total knockdown of all Drp1 transcripts (siDrp1-total) drastically reduced both cellular
372 proliferation and migration, indicating a differential response to total Drp1 perturbation and
373 variant-specific knockdown. The increased cell proliferation and migration observed with high
374 Drp1(-/17):low Drp1(16/17) expression upon variant-specific knockdown emphasizes the pro-
375 tumorigenic capacity of the Drp1(-/17) variant. These findings echo TCGA data, where poorer
376 patient survival was associated with low Drp1(16/17):high Drp1(-/17) ratios. The above findings
377 also emphasize the importance of the expression ratio between the Drp1(16/17) and Drp1(-/17)
378 variants. This is evidenced by the observation that a combined knockdown of Drp1(-/16) and
379 Drp1(-/-), reflecting an equal expression (50:50) of Drp1(16/17) and Drp1(-/17), led to relatively
380 minor changes in mitochondrial morphology, with no significant impact on mitochondrial
381 function, cellular proliferation, or migration. Taken together, these data validate our previous
382 observations from the overexpression of the Drp1(-/17) and Drp1(16/17) variants, and they
383 emphasize the importance of maintaining a balanced ratio of expression between these two
384 variants for optimal mitochondrial morphology and function as this balance may play a critical
385 role in cancer progression.

386

387 **Discussion**

388 To our knowledge this is the first description of Drp1/*DNM1L* transcript variants and their
389 functional significance in a pathophysiological setting. While Drp1 has been extensively studied
390 in various diseases, including multiple cancers [12, 14, 44-46], the investigation of different Drp1
391 isoforms arising from alternate splicing has remained limited, with few studies conducting direct
392 comparisons [26, 27, 29, 32, 47]. Moreover, prior research has often neglected to specify which Drp1
393 isoform was the subject of study. It is assumed that studies investigating the function of Drp1 in
394 cancer cells utilized plasmid that contains all exons of the variable domain (i.e., Drp1(16/17)) to
395 overexpress recombinant Drp1, or that knock-down strategies targeted the expression of all
396 Drp1 variants. Given our findings that alternate splicing of exon 16 is an important feature of
397 ovarian cancer that is associated with poor patient outcome, and that alternate splicing of exon
398 16 results in expression of 2 *DNM1L*/Drp1 proteins with distinct function related to regulation of

399 mitochondrial form and function, future studies focused on Drp1 should take expression and
400 function of *DNM1L*/Drp1 splice variants into consideration.
401 According to TCGA data the *DNM1L* gene is amplified in >50% serous ovarian cancer
402 cases (5% high level amplification, 46% low level gain), while only 7% of cases show
403 heterozygous loss (Extended Data Fig.2e). Published work has correlated *DNM1L* amplification
404 with enhanced cell cycle gene expression and poor survival in chemo-resistant and recurrent
405 cancer samples [12, 31]. Notably, previous analyses of mRNA expression did not discern levels of
406 specific Drp1 splice variants, leaving it uncertain which transcripts are associated with cell cycle
407 gene expression, prognosis, and chemoresistance. We found that ovarian cancer cells derived
408 from patient ascites, as well as TCGA ovarian cancer specimens predominantly express a
409 transcript lacking exon 16 [Drp1(-/17)]. Strikingly, high Drp1(-/17) expression correlates with
410 poorer overall patient survival. This identification of a specific Drp1 splice variant linked to
411 unfavorable patient outcomes holds crucial clinical implications. It suggests that Drp1(-/17)
412 expression confers advantages to ovarian cancer cells, making the relative expression of Drp1(-
413 /17) versus Drp1(16/17) a predictive marker for outcomes. Moreover, it underscores the clinical
414 impact of Drp1 splice variant expression in ovarian cancer for the first time.
415 We established that the two major ovarian cancer Drp1 splice variants, Drp1(-/17) and
416 Drp1(16/17) have distinct localization and effects on mitochondrial morphology and function.
417 Drp1(-/17) variant was previously reported to localize to microtubules, and this association
418 shown to consequently result in decreased fission activity compared to Drp1(16/17)[27]. Similarly,
419 we observed that Drp1(-/17) associated more frequently with microtubules, rather than
420 mitochondria compared to Drp1(16/17). This decrease in mitochondrial association likely
421 explains why Drp1(-/17) expression shifts mitochondrial morphology towards a fused state.
422 Importantly, through splice-specific knockdown of Drp1 variants, we provide the first validation
423 of the fusion phenotype associated with Drp1(-/17) at endogenous expression levels. The
424 variant specific knockdowns also emphasize the significance of stoichiometric expression of the
425 Drp1 splice variants in fine tuning regulation of mitochondrial morphology, possibly representing
426 a novel mechanism exploited by cancer cells to manipulate their mitochondrial dynamics and
427 subsequently mitochondrial function.
428 Decreased fission, and a consequentially more fused mitochondria network has been
429 shown to enhance electron transport chain super-complex assembly and to improve
430 mitochondrial respiratory function[39, 48]. We demonstrated that Drp1(-/17) expression is
431 associated with enhanced mitochondrial respiratory function and more compact cristae
432 arrangement potentially enabling cancer cells to thrive under stress when heightened

433 mitochondrial function is necessary. Stress-induced mitochondrial hyperfusion has been shown
434 to confer resistance to subsequent insults, promoting cell survival[35, 49, 50]. Similarly, the fused
435 networks resulting from elevated Drp1(-/17) expression likely allow ovarian cancer cells to
436 bolster mitochondria robustness and maintain metabolic efficiency.
437 Numerous investigations have emphasized the significance of dynamically adapting
438 mitochondrial morphology, as it plays a pivotal role in metabolic flexibility and cell survival in a
439 context-dependent manner [35, 49-53]. Furthermore, the preference for metabolic fuels is closely
440 associated with mitochondrial architecture[53-55]. Indeed, our study not only establishes altered
441 mitochondrial function associated with Drp1 variant expression but also unveils subsequent
442 metabolic reprogramming in these cells, illustrating the connection between mitochondrial
443 morphology and metabolic adaptability driven by these splice variants. The profile of total
444 metabolites in cells expressing Drp1(-/17) underscores a notably active metabolic phenotype,
445 characterized by elevated glycolysis and TCA cycle metabolites. Recent research highlights that
446 cancer cells derive energy not solely from glycolysis but also from mitochondrial respiration [56, 57].
447 Additionally, ovarian cancer stem cells and chemoresistant cells exhibit a remarkably adaptable
448 metabolic phenotype, capable of switching between glycolysis and oxidative phosphorylation
449 depending on which pathway confers a selective growth advantage and chemoresistance[30, 35, 52,
450 56, 58-60]. Moreover, metabolic alterations are essential to sustain unbridled growth in cancer cells,
451 with increased ATP synthesis and a shift towards de novo macromolecule biosynthesis. While
452 the increased mitochondrial networking observed in Drp1 (-/17) and cristae architecture
453 potentially contributes to ETC complex assembly and efficiency in oxidative phosphorylation, the
454 observed increase in TCA cycle metabolites suggestive an increase in TCA cycle flux, which
455 could be driven by the need for NADH reducing equivalents, as demonstrated by increased
456 levels of NADH in Drp1 (-/17) cells. It remains to be determined if mitochondrial architecture
457 also contributes to the activity or efficiency of TCA cycle enzymes, although it is known that
458 substrate availability is enhanced by a more fused mitochondrial network [36, 39].
459 Prior metabolic profiling of ovarian cancer cells and tumors derived from patients has
460 revealed discernible differences in purine and pyrimidine metabolism, glycerolipid metabolism,
461 and energy metabolism [59, 61, 62] Interestingly, akin to earlier observations in ovarian cancer
462 tumors compared to borderline cases, Drp1(-/17) expression correlated with heightened levels
463 of amino acids like glutamine, glycine, and aspartate, all crucial components for purine and
464 pyrimidine metabolism. Furthermore, the decreased serine levels and increased glycine levels
465 associated with Drp1(-/17) expression suggest enhanced catabolism of the nonessential amino
466 acid serine through the mitochondrial one-carbon unit pathway, essential for purine nucleotide

467 synthesis. This underscores the potential of Drp1(-/17) expression to enable ovarian cancer
468 cells to elevate mitochondrial fidelity, potentially granting greater metabolic flexibility in the face
469 of shifting nutrient availability and conferring survival advantages when subjected to metabolic
470 selection pressures during tumor progression.

471 Another significant observation is that the diminished fission accompanied by Drp1(-/17)
472 expression leads to enhanced cell survival, proliferation, and increased resistance to apoptosis.
473 This implies a potential advantage for these cells under chemotherapeutic pressures. Drp1 has
474 been extensively studied as a regulator of cell death and proliferation. On one hand, Drp1-
475 mediated fission is crucial for mitosis in cancer cells [14, 15], while on the other hand, fragmented
476 mitochondria hinder the G1-S transition in cells, which is linked to the accumulation of cyclin E
477 and a hyperfused mitochondria [63]. Similarly, elevated mitochondrial fusion has been identified
478 as a feature of ovarian cancer neoplastic stem cells, priming them for self-renewal and
479 proliferation [64]. We predict these conflicting reports related to Drp1 expression and cell
480 proliferation might be partially resolved by considering Drp1 variant expression. Especially as
481 our findings with splice variant specific Drp1 knockdown show distinct impact of Drp1 variants
482 on cell proliferation, with Drp1(-/17) variant primarily associated with enhanced cell survival and
483 proliferation.

484 Furthermore, since Drp1-mediated mitochondrial fission is essential for initiating
485 apoptosis, the lack of coordinated fission and the resultant fused mitochondria in Drp1(-/17)
486 expressing cells could account for the observed resistance to apoptosis upon exposure to
487 agents like cisplatin and paclitaxel. We propose that this heightened resistance to
488 chemotherapy, coupled with the survival advantages conferred by improved mitochondrial
489 function, contribute to the poorer outcomes observed in patients with high tumor expression of
490 Drp1(-/17). Intriguingly, previous reports on chemoresistant ovarian cancer cells indicate a
491 higher abundance of tubular and elongated mitochondria, potentially suggesting that enhanced
492 fusion could be a mechanism through which tumors evade apoptosis [65, 66]. Given the unique
493 association of Drp1(-/17) with microtubules, the target site of taxanes, further investigations are
494 warranted to ascertain whether the heightened chemoresistance conferred by Drp1(-/17) is
495 attributed to reduced mitochondrial fission or its interaction with microtubules. The interaction of
496 Drp1 with microtubules was previously shown to be driven by direct, electrostatic interactions
497 between the conserved basic residues in Drp1 exon 17 (Arg566/567) and the acidic N-termini of
498 α/β-tubulin. The existence of exon 16 in the Drp1(16/17) sequence is hypothesized to impede
499 this interaction, possibly by physically obscuring or neutralizing the positive charge of the
500 neighboring microtubule binding domain [27]. Future work is needed to elucidate potential extra

501 mitochondrial function of Drp1(-/17) and how these could be additionally contributing not only to
502 the abrogated fission activity of this protein, but other cellular functions that play a role in driving
503 the enhanced tumorigenic features of cells predominantly expressing this variant.
504 While our work focused on ovarian cancer, the importance of Drp1 splice variants in
505 other tumor types requires further investigation. Other shortcomings of this work that require
506 further investigation are the lack of understanding as to why and how exon 16 is specifically
507 spliced out in ovarian cancer cells. While cancer cells in general are known for their alterations
508 in RNA splicing and processing [47, 67, 68] it remains to be determined if specific alterations in the
509 RNAs splicing machinery give rise to higher expression of Drp1(-/17). As such, aberrant
510 expression of RNA splice factors such as SRSF3 is associated with ovarian cancer [69, 70].
511 In summary, our study sheds light on the pathophysiological importance of Drp1 variant
512 expression and their ability to modify mitochondrial fission and fusion dynamics as a novel
513 mechanism underlying ovarian cancer cell plasticity. This study also emphasizes the necessity
514 of expanding our comprehension of these Drp1 splice variants, potentially beyond the scope of
515 cancer, and their consideration in future investigations on the function of Drp1 in different
516 (patho)physiological settings.
517

518 **Materials & Methods**

519 *Cell lines and cell culture*

520 Cell lines were generously provided by the following investigators: OVCA433, OVCA420 Dr.
521 Susan K. Murphy; HeyA8, Dr. Katherine Aird; FT282, Dr. Ronny Drapkin. ES-2, TOV-21-G and
522 OVCAR3 cells were purchased from American Type Culture Collection (ATCC, CRL-1978, HTB-
523 161). OVCA433, OVCA420, SKOV3 and HeyA8 cells were cultured in RPMI 1640 medium
524 (Corning,10-040-CV) supplemented with 10% fetal bovine serum, FBS (Avantor®
525 Seradigm,1500-500). OVCA433 and SKOV3 cells under selection were maintained in fully
526 supplemented growth media with 5ug/ml Puromycin (Gibco™, A1113803). OVCAR3 cells were
527 cultured in RPMI1640 medium supplemented with 0.01 mg/ml bovine insulin (Fisher Scientific,50-
528 608-896) and 10% FBS ES-2 cells were cultured in Modified McCoy's 5a Medium (Corning,10-
529 050-CV) with 10% FBS. TOV-21-G cells were cultured in a 1:1 mix of MCDB 105 (Sigma-
530 Aldrich,117-500) containing 1.5 g/L sodium bicarbonate (Gibco™,25080094) and Medium 199
531 (Corning,10-060-CV) containing 2.2 g/L sodium bicarbonate, with 15% FBS. FT282 cells were
532 cultured in 50% DMEM and 50% Ham's F-12 medium (Corning,10-090-CV) supplemented with
533 2% FBS. All cells were maintained at 37°C with 5% $CO_2$. Cell lines were routinely tested for

534 Mycoplasma contamination using EZ-PCR™ Mycoplasma Detection Kit (Captivate Bio,20-700-
535 20). Cell line authentication was carried by STR genotyping (Labcorp).
536
537 *Patient ascites derived EOC cells.*
538 Epithelial Ovarian Cancer (EOC) cells were isolated from malignant ascites of ovarian cancer
539 patients treated at the Women's Cancer Care clinic (Albany, NY) and the Penn State Hershey
540 College of Medicine Division of Gynecologic Oncology, with approval granted from the State
541 University of New York at Albany and the Penn State College of Medicine IRBs. Histological
542 subtype and staging of EOC samples shown in Fig. 2c. Following procurement of ascites EOCs
543 were immediately isolated and cultured as previously described[71], and maintained in culture at
544 37°C, 5% $CO_2$ in MCDB/M199 medium supplemented with 10% FBS and penicillin/streptomycin.
545
546 *Matched tumor specimens*
547 Archival matched specimens of normal fallopian tube or ovary, ovarian tumor and omental
548 tumor from high grade serous ovarian cancer patients were obtained through an honest broker
549 from the ProMark biospecimens bank at the University of Pittsburgh Magee Womens Research
550 Institute, with approval granted from the University of Pittsburgh IRB. Histological subtype and
551 staging of tumor specimens shown in Extended Fig. 3b.
552
553 *5'/3' Rapid amplification of cDNA ends (RACE)*
554 3' and 5'RACE reactions were carried out using the SMARTer 3'5' RACE kit (Takara),
555 essentially as recommended by the manufacturer. 5'RACE was carried out with the Universal
556 Primer A Mix (UPM) and the *DNM1L* specific antisense primer, positioned in Exon 12: 5'
557 GTTCCACACAGCGGAGGCTGGGC 3'. 3'RACE was carried out using *DNM1L* primer
558 spanning the exon junction of exon 6/7: 5'
559 GATTACGCCAAGCTTTGCCAGGAATGACCAAGGTGCCTGT-3', followed by nested PCR on
560 the PCR product using *DNM1L* specific primers in exon 10/11: 5'
561 GATTACGCCAAGCTTACTTCGGAGCTATGCGGTGGTGCT-3'. RACE PCR products were
562 resolved on a 10% agarose gel, bands gel purified and cloned into the pRACE vector for
563 subsequent sequencing of inserts. Poly A sites were annotated to the *DNM1L* gene using the
564 NCBI genome browser tracks for PolyA sites and clusters, Polyadenylation sits from PolyA_DB
565 (v.3.2) and the polyadenylations sites from the PolyASites at the University of Basel.
566
567 *Drp1/DNM1L variant RT-PCR*

568 Total RNA from cells and tissue was isolated using Direct-zolTM RNA Miniprep kit (Zymo
569 Research, R2052). Prior to RNA purification tissue was crushed under liquid Nitrogen and 25-50
570 mg of tissue-powder lysed in 800ml Ambion TRIzol Reagent (Invitrogen™,15596018) overnight
571 at 4$^{o}$C. First-strand cDNA synthesis was performed using qScript cDNA Synthesis Kit
572 (Quantabio, 95047) according to the manufacturer's instruction. RT-PCR was performed using
573 diluted cDNA (1:5 in water) and PrimeStar DNA Polymerase (Takara, R010A) with primers and
574 PCR conditions listed in Table 1. The amplified products, mixed with Gel Loading Buffer II
575 (Thermo Scientific,AM8547), were separated on a PA-TBE gel and stained with GelStarTM
576 Nucleic Acid Gel Stain (Lonza, 50535).

| Primer | Sequence (S: sense; AS: antisense) | PCR Cycle |
|---|---|---|
| Drp1 Variable Domain Variants (Exons 16/17) | S: 5'-GGCAATTGAACTGGCTTATATCAACAC-3'<br>AS: 5'-TGGTTGGTTCTTGAACACCATCTCCAA-3' | 98C-15s,<br>(98C-10s, 70C-15s, 72C-20s) X32 |
| Drp1 ΔC truncated Variants | S: 5'-GGCAATTGAACTGGCTTATATCAACAC-3'<br>AS: 5'-TAGATA CCACTACACAAACAGGTTCTT-3' | 98C-15s,<br>(98C-10s, 70C-15s, 72C-20s) X32-40 |
| Total Drp1 (Exons 1-2) | S: 5'-GTGGGCCCCGGCCCCATTCAT-3'<br>AS: 5'- CAGTACCTCTGGGAAGCAGGTCCCTCC-3' | 95C-3m,<br>(95C-10s, 68C-15s, 72C-20s) X32 |
| Actin | S: 5'-AACTGGGACGACATGGAG-3'<br>AS: 5'- TAGCACAGCCTGGATAGCAACGTA-3' | 98C-15s,<br>(98C-10s, 70C-15s, 72C-20s) X24 |

577

578 *siRNA-mediated knock-down*

579 Cells were transfected with scramble non-targeting SMARTpool control (Dharmacon#D-001810-
580 10-05) or single or combination of Drp1 variant specific siRNA oligonucleotides against target
581 sequence listed in Table 2 using Lipofectamine RNAiMAX (Invitrogen, 13778150). 48 hours
582 post-transfection cells were seeded for experiments. For each experiment, knock-down was
583 confirmed by RT-PCR using Drp1 variable domain variant RT-PCR primers, as above.

| Drp1 siRNA | Target Sequence - 5'-3' | Target location |
|---|---|---|
| siDrp1(total) | GAGAAACAGGCTAGCCAGAGAATTACCTTCA | Exon 15 |
| siDrp1(16/17) | GAGGCTGATGGCAAGTTAATTCAGGACAGCA | Exon 16/17 junction |
| siDrp1(-/17) | CTGTATCACGAGACAAGTTAATTCAGGACAG | Exon 15/17 junction |
| siDrp1(16/-) | GAGGCTGATGGCAAGGTTGCATCTGGAGGTG | Exon 16/18 junction |
| siDrp1(-/-) | CTGTATCACGAGACAAGGTTGCATCTGGAGG | Exon 15/18 junction |

584

585 *Immunoblotting*

586 Cells were cultured to sub-confluency and lyzed in RIPA buffer (Thermo Scientific™, 89901)
587 containing protease and phosphatase inhibitors (Thermo Scientific™, 78443). The protein
588 supernatant was collected following 30 mins rotation at 4°C, followed by maximum speed
589 (21,000 rcf) centrifugation for 30 mins in a 1.5 ml tabletop centrifuge at 4°C. Protein
590 concentrations were measured using the Pierce BCA protein assay kit (Thermo Scientific™,
591 23225). Following SDS-PAGE, proteins were transferred to PVDF membranes. Membranes
592 were blocked for an hour in in 5% non-fat milk (Bio-Rad,1706404)/TBS, 0.1% Tween20
593 (MilliporeSigma, 900-64-5) and were probed overnight at 4°C in primary antibodies. The next
594 day blots were incubated for 1 hour at room temperature with horseradish peroxidase (HRP)-
595 conjugated secondary antibodies and were developed using SuperSignal™ West Femto
596 Maximum Sensitivity Substrate Femto (Thermo Scientific™, 34096).
597 *Antibodies used:*

| Antibody | Manufacturer | Cat # | Dilution |
|---|---|---|---|
| Drp1 | abcam | 184247 | 1:1000 |
| Drp1 | EMD Millipore | ABT155 | 1:1000 |
| Drp1/DLP1 | BD Transduction | 611112 | 1:1000 |
| Phospho-DRP1 (Ser616) | Cell Signaling | 3455 | 1:1000 |
| MitoBiogenesis™ Western Blot Cocktail | abcam | 123545 | 1:250 |
| β-actin (9f3) | Thermo Scientific | AM4302 | 1:1000 |
| β-tubulin (AC-15) | Cell Signaling | 2128 | 1:1000 |
| GAPDH (0411) | Santa Cruz | sc-47724 | 1:1000 |
| Vinculin | Sigma-Aldrich | Aldrich V9131 | 1:1000 |
| Amersham ECL HRP conjugated rabbit IgG | Cytiva | NA934 | 1:10000 |
| Amersham ECL HRP conjugated mouse IgG | Cytiva | NA931 | 1:10000 |

598
599 *TCGA data analysis*
600 RNAseq bam files for the TCGA serous ovarian carcinoma cohort (n = 379, all cases regardless
601 of grade and stage) were downloaded from dbGaP and stored on a secure server according to
602 dbGaP protocols. The samtools 1.9.0 software [72] was used to convert each bam file to two
603 fastq files corresponding to the paired end reads after randomizing the order of the reads with
604 'samtools collate.' The salmon 1.3.0 software [73] was then applied to quantify genome-wide

605 transcript abundances based on an index created from a custom reference fasta file, as
606 described below, that incorporates sequences from splice variants and alternate
607 polyadenylation forms of DNML1. The --seqBias, --gcBias, and --validateMapping options for
608 the salmon quant command were utilized. The salmon index was created by following the steps
609 outlined at https://combine-lab.github.io/alevin-tutorial/2019/selective-alignment/. First, a
610 decoys.txt file was created using the GRCh38 primary assembly fasta file. Next, a custom
611 version of the gencode.v22.pc_transcripts.fa file was made by removing all transcripts
612 corresponding to the DNML1 gene and replacing them with sequences corresponding to the
613 alternate splice and alternative polyadenylated transcripts of *DNML1*. Concatenating this
614 custom transcriptome fasta file with the GRCh38 primary assembly fasta file yielded the
615 gentrome fasta file that, along with the decoys.txt file, was used to produce the salmon index.
616 Overall survival data was obtained using cBioportal.
617
618 *Drp1 plasmids & subcloning*
619 Rat Drp1(-/17) and Drp1(16/17) cloned in pEGFP-C1 plasmids were kindly provided by Dr.
620 Stefan Strack, University of Iowa [27]. Drp1 coding sequence were subcloned into pLenti-CMV-
621 MCS-GFP-SV-puro (Addgene, 73582) with a N-terminal GFP tag and sequenced to confirm
622 successful cloning of Drp1(-/17) and Drp1(16/17) plasmids. The plasmids were transfected in
623 293-FT cells for expression and lentiviral particle production. OVCA433 and SKOV3 cells were
624 infected and transduced with the GFP vector control, GFP-Drp1(-/17) and GFP-Drp1(16/17)
625 virus, selected for expression using 5ug/ml Puromycin for 1-2 weeks and sorted for GFP
626 expression by flow cytometry to generate stable Drp1 overexpressing cells.
627
628 *Immunofluorescence and analysis of mitochondrial morphology*
629 Prior to imaging, mitochondria were labelled in cells by transduction with pLV-mitoDsRed virus
630 (Addgene, Plasmid 44386) harvested post expression in 293-FT cells and lentiviral particle
631 production. For imaging, cells were seeded at 60-70% confluency in Chambered Cell Culture
632 slides (Falcon, 08-774-25). Next day, cells were washed once with 1X PBS (Corning, 21-040-
633 CV) and fixed in 4% formaldehyde, made fresh by diluting 16% PFA solution (BTC BeanTown
634 Chemical,30525-89-4) in 1X PBS for 10 mins at room temperature. For imaging FCCP
635 treatment, cells were incubated with 1μM FCCP(Sigma) in media for 30 mins prior to fixation.
636 Post fixation, cells were rinsed twice with 1X PBS and permeabilized for 10-15 mins using 0.2 %
637 Triton™ X-100 (Fisher Scientific, BP151500) in 1X PBS with gentle rocking. Followed by two
638 more PBS rinses prior to 1 hour incubation with SuperBlock™ Blocking Buffer (Thermo

639 Scientific™,37515) for blocking non-specific antibody binding. Cells were stained with primary
640 antibody against Tubulin (Abcam, ab6160) at 1:1000 dilution in SuperBlock™ blocking buffer for
641 either 1hr 30 mins at room temperature or overnight at 4°C. After incubation cells were washed
642 for three subsequent 10 min washes with 1X PBS with gently rocking. Cells were incubated with
643 1:1000 dilution of secondary rat antibody conjugated with Alexa Fluor® 647 (abcam, 150167) in
644 SuperBlock™ Blocking Buffer at room temperature for 30 mins. After, washed with 1X PBS for
645 three times,10 mins each to remove any residual antibody. Slides were mounted in ProLong™
646 Gold Antifade Mountant with DNA Stain DAPI (Invitrogen™, P36935) and dried overnight in
647 dark at room temperature. For mitochondrial imaging of SKOV3 post siRNA transfection, cells
648 were seeded on 35mm glass bottom dishes (MatTek, P35GC-1.5-14-C). Next day cells were
649 stained using MitoTracker™ Green FM (Invitrogen™, M7514) following the manufacturer's
650 recommendations. Briefly, cells were incubated for 12-15 mins in pre-warmed culture medium
651 containing 250 nM MitoTracker™ Green FM and Hoechst 33342 (Thermo Scientific™,62249).
652 After, cells were washed thrice with 1X PBS and imaged in pre-warmed 1X HBSS (Corning, 21-
653 023-CV). Z-stacks were taken with Leica Thunder Imager using 63X oil immersion objective and
654 subjected to inbuilt thunder de-convolution. The mitochondrial network morphology to look at the
655 elongation and fragmentation was performed on 2D Z-stack projections in image J using the
656 mitochondria-analyzer plugin (https://github.com/AhsenChaudhry/Mitochondria-Analyzer).
657 Briefly, the images were converted into binary, and threshold was adjusted to detect the
658 mitochondrial network before performing the 2D per-cell mitochondrial network analysis. Total of
659 at least 150 or more cells were analyzed to get the morphological network parameters with 30
660 cells or more. analyzed for each biological replicate over at least 3 or more biological replicates.
661 Representative images shown were adjusted in brightness and contrast for better visualization.
662
663 *TEM*
664 Cells were fixed in cold 2.5% glutaraldehyde (25% glutaraldehyde stock EM grade,
665 Polysciences, 111-30-8) in 0.01 M PBS (Fisher), pH 7.3. Samples were rinsed in PBS, post-
666 fixed in 1% osmium tetroxide (Electron Microscopy Sciences) with 1% potassium ferricyanide,
667 (Fisher), rinsed in PBS, dehydrated through a graded series of ethanol, and embedded in
668 Poly/Bed® 812 (Luft formulations). Semi-thin (300 nm) sections were cut on a Reichart Ultracut
669 (Leica Microsystems), stained with 0.5% Toluidine Blue O (Fisher) in 1% sodium borate (Fisher)
670 and examined under the light microscope. Ultrathin sections (65 nm) were stained with 2%
671 uranyl acetate (Electron Microscopy Science) and Reynold's lead citrate (Lead Nitrate, Sodium
672 Citrate and Sodium Hydroxide, Fisher) and examined on JEOL 1400 Plus transmission electron

673 microscope with a side mount AMT 2k digital camera (Advanced Microscopy Techniques). For
674 morphometric analysis of mitochondria by transmission electron microscopy, mitochondrial
675 area, mitochondrial length (major axis), cristae number and cristae volume density per
676 mitochondria was quantified and analyzed as described[74] using ImageJ. At least 40-50
677 mitochondria per biological replicate over 3 experimental replicates were analyzed.

678 *TMRE Protocol*

679 OVCA433 and SKOV3 were seeded into 96-well plates at a density of 1,000 cells per well and
680 incubated overnight in a cell culture incubator at 37ºC and 5% $CO_2$. The following day, half the
681 sample wells were treated with 10 µM FCCP and incubated for 30 minutes in a cell culture
682 incubator. All the sample wells were then treated with 100 nM TMRE (Thermo Fisher Scientific,
683 T669), and incubated for 30 minutes at 37ºC in a cell culture incubator. All samples were
684 subsequently washed twice with 1X PBS, and fluorescence measurements were taken with a
685 Synergy HT microplate reader (BioTek) with an excitation wavelength of 530 nm and emission
686 wavelength of 590 nm.
687

688 *MitoSox mitochondrial superoxide indicator*

689 500,000 cells were stained with 5 µM MitoSOX Red mitochondrial superoxide indicator
690 (Invitrogen, M36008) in 1 ml HBSS (Corning, 21-023-CV) for 30 minutes at 37ºC. Following
691 incubation, cells were washed with HBSS, and florescence was measured using flow cytometry
692 as per manufacture's protocol. Unstained cells were used as a negative control while cells
693 treated with 50 µM Antimycin A were used as a positive control for flow cytometry.
694

695 *Bioenergetic Analysis of Oxygen Consumption Rate (OCR) and Extracellular Acidification Rate*
696 *(ECAR)*

697 The Agilent Seahorse XFp Metabolic Analyzer (Agilent, model S7802A) was used to assess
698 mitochondrial respiration of OVCA433 and SKOV3 as described previously for attached cells[75].
699 Briefly, prior to the start of the experiment, cells were evenly seeded and cultured overnight in a
700 Seahorse XFp cell culture plate (Agilent, 103022-100) at a density of 10,000 and 8,000
701 cells/well for OVCA433 and SKOV3, respectively. The XFp sensor cartridge was hydrated in
702 Agilent Seahorse XF Calibrant (Agilent,103022-100) at 37°C in a humidified incubator (non-
703 $CO_2$) incubator overnight. On the day of the experiment, cell culture media was replaced with
704 pre-warmed seahorse XF base RPMI media, pH 7.4 (Agilent,103576-100) supplemented with 1
705 mM sodium pyruvate (Agilent 103578-100), 2 mM glutamine (Agilent 103579-100), and 10 mM
706 glucose (Agilent, 103577-100). Cells were then placed into a non-$CO_2$ humidified incubator at

707 37°C for 60 min. Mitochondrial stress test reagents (pharmacological manipulators of
708 mitochondrial respiratory chain proteins) were diluted in pre-warmed XF assay media to achieve
709 the following final concentrations in the cell culture well: 1.5 μM Oligomycin A (Sigma, 75351); 1
710 or 0.5 μM FCCP (Sigma, C2920) for OVCA433 and SKOV3, respectively; and 0.5 μM Antimycin
711 A/Rotenone (Sigma, A8674,45656). Three basal rate measurements (3 min measurement time
712 each) were taken prior to the injection of mitochondrial stress test reagents and three
713 measurements of OCR/ECAR were obtained respectively following injection of compounds.
714 Post-run, the cells were stained with crystal violet dye (0.05%) (Sigma-Aldrich, 229288) for
715 seeding normalization. The dye was released from cells using 30% acetic acid and absorbance
716 was measured at 590 nm, using GloMax Explorer (Promega) microplate reader.
717
718 *Metabolomics*
719 1-2 million cells were seeded in 60 mm dishes per replicate (n=6 for each condition) in normal
720 cell growth media. Next day, cells were washed once with 1X PBS and fresh media was added.
721 After 24 hours, metabolic quenching and polar metabolite pool extraction was performed by
722 adding ice cold 80% methanol (aqueous with 0.1% formic acid) at a ratio of 500μL buffer per
723 1e6 cells. Deuterated (D3)-creatinine and (D3)-alanine, (D4)-taurine and (D3)-lactate (Sigma-
724 Aldrich) was added to the sample lysates as an internal standard for a final concentration of
725 10μM. Samples are scraped into Eppendorf tubes on ice, homogenized using a 25°C water
726 bath sonicator and the supernatant was then cleared of protein by centrifugation at 16,000xg.
727 2μL of cleared supernatant was subjected to online LC-MS analysis. Analyses were performed
728 by untargeted LC-HRMS. Briefly, Samples were injected via a Thermo Vanquish UHPLC and
729 separated over a reversed phase Thermo HyperCarb porous graphite column (2.1×100mm,
730 3μm particle size) maintained at 55°C. For the 20 minute LC gradient, the mobile phase
731 consisted of the following: solvent A (water / 0.1% FA) and solvent B (ACN / 0.1% FA). The
732 gradient was the following: 0-1min 1% B, increase to 15%B over 5 minutes, continue increasing
733 to 98%B over 5 minutes, hold at 98%B for five minutes, reequillibrate at 1%B for five minutes.
734 The Thermo IDX tribrid mass spectrometer was operated in both positive and ion mode,
735 scanning in ddMS2 mode (2 μscans) from 70 to 800 m/z at 120,000 resolution with an AGC
736 target of 2e5 for full scan, 2e4 for ms2 scans using HCD fragmentation at stepped 15,35,50
737 collision energies. Source ionization setting was 3.0 and 2.4kV spray voltage respectively for
738 positive and negative mode. Source gas parameters were 35 sheath gas, 12 auxiliary gas at
739 320°C, and 8 sweep gas. Calibration was performed prior to analysis using the PierceTM

740 FlexMix Ion Calibration Solutions (Thermo Fisher Scientific). Integrated peak areas were then
741 extracted manually using Quan Browser (Thermo Fisher Xcalibur ver. 2.7).
742
743 *$NAD^+$ and NADH level determination*
744 OVCA433 and SKOV3 cells were seeded into flat-bottom 96-well plates at a density of 10,000
745 and 8,000 respectively in normal growth medium. After overnight incubation, total NAD+ and
746 NADH levels and their ratios were determined using NAD+/NADH-glo assay kit (Promega,
747 G9071) as per manufacture's protocol. Following addition of NAD/NADH-GloTM Detection
748 Reagent, samples were incubated for 1 hour at room temperature and transferred to white flat-
749 bottom 96-well plate (BrandTech® ,BRA-781605). Bioluminescence was measured with GloMax
750 Explorer (Promega) plate reader. Protein Concertation was determined by BCA and used for
751 data normalization.
752
753 *Cell proliferation and viability*
754 Equal number of cells were seeded into 96 well plates at density of 1000 and 500 cells/well for
755 OVCA433 and SKOV3 respectively, in normal culture medium. For cell proliferation rate, cell
756 numbers were analyzed for 3 days successively using FluoReporter™ Blue Fluorometric dsDNA
757 Quantitation Kit (Invitrogen™, F2962) as per manufacturer's protocol and fluorescence
758 measurements were taken with a Victor X (PerkinElmer) microplate reader with an excitation
759 wavelength of 360 nm and emission wavelength of 460 nm respectively. Proliferation rate was
760 measured as the increase in the cell density relative to day 1. For cell viability in response to
761 chemotherapeutic agents, cells were treated with indicated doses of Cisplatin (cis-
762 Diamineplatinum(II) dichloride) (Sigma) or Paclitaxel(Sigma). Following 72 hours of drug
763 treatment cell viability was measured using FluoReporter™ Blue Fluorometric dsDNA
764 Quantitation Kit and was expressed as percentage survival relative to non-treated cells.

765 *Caspase 3/7 activity assay*

766 OVCA433 and SKOV3 cells were seeded into flat-bottom 96-well plates at a density of 7,000
767 and 5,000 cells per well respectively in normal growth medium. After overnight incubation, cells
768 were treated with 5 μM Cisplatin (cis-Diamineplatinum(II) dichloride) (Sigma) or 1 nM
769 Paclitaxel(Sigma) respectively. After 24 hours drug treatment, caspase 3/7 activity was
770 measured using Caspase-Glo® 3/7 Assay System- (Promega, G8091) per manufacture's
771 protocol. Briefly, equal volume of reagent was added to the samples and only media control.
772 Following 1 hour incubation in dark at room temperature, samples were transferred to white flat-

773 bottom 96-well plate (BrandTech® ,BRA-781605) and bioluminescence was measured with
774 GloMax Explorer (Promega) plate reader.

775 *Clonogenicity assay*
776 100 cells/well were seeded in a 6 well plate for single cell survival clonogenicity assay and
777 cultured for 7-10 days under normal culture conditions. Clonogenicity was assessed by staining
778 colonies with crystal violet (0.05%). Colonies were counted using Image J and data expressed
779 as cellular survival fraction.
780
781 *Migration Assay*
782 For assessment of Transwell migration, cell culture inserts (Corning, 353097) with 8.0 µm
783 Transparent PET Membrane, were each placed into a 24- well plate with 800 µL complete
784 growth medium (with serum) added at the bottom of each well. 50,000 and 30,000 cells of
785 OVCA433 and SKOV3, respectively were seeded onto the top of the Transwell membrane of
786 the insert in 150 µL serum free media. After 24 hours, the Transwelll inserts were removed and
787 washed twice with 1XPBS. The Transwell membrane was fixed and stained with Crystal violet
788 (0.05%) for an hour. The inserts were washed three times with 1X PBS and the non-migrated
789 cells were removed from the top of the membrane using dry cotton swabs. The inserts were
790 dried overnight, and images were taken of the migrated cells at the bottom of the membrane
791 using Leica Thunder Imager with colored K3C camera. The dye was released from cell inserts
792 using 30% acetic acid and absorbance was measured using GloMax Explorer (Promega)
793 microplate reader at 590 nm as a readout for cell migration.
794
795 *Data and Statistical Analysis*
796 All data presented are from at least three biological replicates and represented as mean ±
797 standard error of the mean. Unless otherwise indicated, statistical data analysis was carried out
798 using GraphPad Prism Software (10.0.2), with appropriate analyses chosen based on
799 experimental design, as stated in figure legends.
800

801 **Acknowledgements**

802 The authors would like to thank Dr. Stefan Strack for providing Drp1 splice variant plasmids. We
803 would like to thank the following individuals for helpful scientific discussions: Yisang Yoon,
804 Janine Santos, Patrick Kimes. We thank Royden Clark, Emmy Dier, Sara Shimko and Ben
805 Yankasky for technical assistance. This work was supported by the U.S. Department of Defense

CDMRP pilot award W81XWH-16-1-0117, TEAL award W81XWH-22-10252 and NIH R01CA242021 (to N.H.), R01CA230628 (to K.M. & N.H), NIH training grant 2T32HL110849-11A1 (to S.W.), R35-HL150778 (to M.T.), NIHS10OD023402 (to S.L.G.) and NIH instrumentation grants S10RR025488, S10RR016236, S10RR019003 (to S.C.W.). Lauren Borho and Dr. Francesmary Mudugno kindly assisted as honest brokers to access patient specimens. The ProMark tissue bank is supported by NIH SPORE P50CA272218.

## Author contributions

Z.J. contributed to conceptual and experimental design, carried out experiments and data analysis, prepared figures and wrote the manuscript. D.H.S contributed to experimental design, carried out experiments and data analysis. W.P., S.W., A.E., S.K., Y.-Y.C., J.C.B., A.E.A., M.S., S.J.M., carried out experiments and performed data analysis. R.P., H.G.W., S.Y., S.C.W., S.G.W., N.L., L.C., K.A. contributed to conceptual ideas and manuscript editing. M.T., V.W., and K.M. contributed to conceptual and experimental design, data analysis and interpretation, and manuscript editing. N.H. supervised and conceived the study, contributed to conceptual and experimental design, assisted in data analysis, writing and editing of the manuscript.

## Conflict of interest

The authors have no conflicts of interest.

## References

1. Kamerkar SC, Kraus F, Sharpe AJ, Pucadyil TJ, Ryan MT. Dynamin-related protein 1 has membrane constricting and severing abilities sufficient for mitochondrial and peroxisomal fission. Nat Commun. 2018;9(1):5239. Epub 2018/12/12. doi: 10.1038/s41467-018-07543-w. PubMed PMID: 30531964; PMCID: PMC6286342.
2. Archer SL. Mitochondrial dynamics--mitochondrial fission and fusion in human diseases. N Engl J Med. 2013;369(23):2236-51. Epub 2013/12/07. doi: 10.1056/NEJMra1215233. PubMed PMID: 24304053.
3. Santel A, Frank S. Shaping mitochondria: The complex posttranslational regulation of the mitochondrial fission protein DRP1. IUBMB Life. 2008;60(7):448-55. Epub 2008/05/10. doi: 10.1002/iub.71. PubMed PMID: 18465792.
4. Yu R, Jin SB, Ankarcrona M, Lendahl U, Nister M, Zhao J. The Molecular Assembly State of Drp1 Controls its Association With the Mitochondrial Recruitment Receptors Mff and

839 MIEF1/2. Front Cell Dev Biol. 2021;9:706687. Epub 2021/11/23. doi:
840 10.3389/fcell.2021.706687. PubMed PMID: 34805137; PMCID: PMC8602864.
841 5. Yamada T, Adachi Y, Iijima M, Sesaki H. Making a Division Apparatus on Mitochondria.
842 Trends Biochem Sci. 2016;41(3):209-10. Epub 2016/02/18. doi: 10.1016/j.tibs.2016.02.001.
843 PubMed PMID: 26879678; PMCID: PMC5378552.
844 6. Cribbs JT, Strack S. Reversible phosphorylation of Drp1 by cyclic AMP-dependent
845 protein kinase and calcineurin regulates mitochondrial fission and cell death. EMBO Rep.
846 2007;8(10):939-44. Epub 2007/08/28. doi: 10.1038/sj.embor.7401062. PubMed PMID:
847 17721437; PMCID: PMC2002551.
848 7. Strack S, Cribbs JT. Allosteric modulation of Drp1 mechanoenzyme assembly and
849 mitochondrial fission by the variable domain. J Biol Chem. 2012;287(14):10990-1001. Epub
850 2012/02/16. doi: 10.1074/jbc.M112.342105. PubMed PMID: 22334657; PMCID: PMC3322891.
851 8. Parone PA, Da Cruz S, Tondera D, Mattenberger Y, James DI, Maechler P, Barja F,
852 Martinou JC. Preventing mitochondrial fission impairs mitochondrial function and leads to loss of
853 mitochondrial DNA. PLoS One. 2008;3(9):e3257. Epub 2008/09/23. doi:
854 10.1371/journal.pone.0003257. PubMed PMID: 18806874; PMCID: PMC2532749.
855 9. Benard G, Bellance N, James D, Parrone P, Fernandez H, Letellier T, Rossignol R.
856 Mitochondrial bioenergetics and structural network organization. J Cell Sci. 2007;120(Pt 5):838-
857 48. Epub 2007/02/15. doi: 10.1242/jcs.03381. PubMed PMID: 17298981.
858 10. Twig G, Elorza A, Molina AJ, Mohamed H, Wikstrom JD, Walzer G, Stiles L, Haigh SE,
859 Katz S, Las G, Alroy J, Wu M, Py BF, Yuan J, Deeney JT, Corkey BE, Shirihai OS. Fission and
860 selective fusion govern mitochondrial segregation and elimination by autophagy. EMBO J.
861 2008;27(2):433-46. Epub 2008/01/18. doi: 10.1038/sj.emboj.7601963. PubMed PMID:
862 18200046; PMCID: PMC2234339.
863 11. Arnoult D, Rismanchi N, Grodet A, Roberts RG, Seeburg DP, Estaquier J, Sheng M,
864 Blackstone C. Bax/Bak-dependent release of DDP/TIMM8a promotes Drp1-mediated
865 mitochondrial fission and mitoptosis during programmed cell death. Curr Biol.
866 2005;15(23):2112-8. Epub 2005/12/08. doi: 10.1016/j.cub.2005.10.041. PubMed PMID:
867 16332536.
868 12. Tanwar DK, Parker DJ, Gupta P, Spurlock B, Alvarez RD, Basu MK, Mitra K. Crosstalk
869 between the mitochondrial fission protein, Drp1, and the cell cycle is identified across various
870 cancer types and can impact survival of epithelial ovarian cancer patients. Oncotarget.
871 2016;7(37):60021-37. Epub 2016/08/11. doi: 10.18632/oncotarget.11047. PubMed PMID:
872 27509055; PMCID: PMC5312366.

873 13. Serasinghe MN, Wieder SY, Renault TT, Elkholi R, Asciolla JJ, Yao JL, Jabado O,
874 Hoehn K, Kageyama Y, Sesaki H, Chipuk JE. Mitochondrial division is requisite to RAS-induced
875 transformation and targeted by oncogenic MAPK pathway inhibitors. Mol Cell. 2015;57(3):521-
876 36. doi: 10.1016/j.molcel.2015.01.003. PubMed PMID: 25658204; PMCID: PMC4320323.
877 14. Kashatus JA, Nascimento A, Myers LJ, Sher A, Byrne FL, Hoehn KL, Counter CM,
878 Kashatus DF. Erk2 phosphorylation of Drp1 promotes mitochondrial fission and MAPK-driven
879 tumor growth. Mol Cell. 2015;57(3):537-51. Epub 2015/02/07. doi:
880 10.1016/j.molcel.2015.01.002. PubMed PMID: 25658205; PMCID: PMC4393013.
881 15. Taguchi N, Ishihara N, Jofuku A, Oka T, Mihara K. Mitotic phosphorylation of dynamin-
882 related GTPase Drp1 participates in mitochondrial fission. The Journal of biological chemistry.
883 2007;282(15):11521-9. Epub 2007/02/16. doi: 10.1074/jbc.M607279200. PubMed PMID:
884 17301055.
885 16. Rehman J, Zhang HJ, Toth PT, Zhang Y, Marsboom G, Hong Z, Salgia R, Husain AN,
886 Wietholt C, Archer SL. Inhibition of mitochondrial fission prevents cell cycle progression in lung
887 cancer. FASEB journal : official publication of the Federation of American Societies for
888 Experimental Biology. 2012;26(5):2175-86. Epub 2012/02/11. doi: 10.1096/fj.11-196543.
889 PubMed PMID: 22321727; PMCID: 3336787.
890 17. Desai SP, Bhatia SN, Toner M, Irimia D. Mitochondrial localization and the persistent
891 migration of epithelial cancer cells. Biophys J. 2013;104(9):2077-88. doi:
892 10.1016/j.bpj.2013.03.025. PubMed PMID: 23663851; PMCID: PMC3647149.
893 18. Wieder SY, Serasinghe MN, Sung JC, Choi DC, Birge MB, Yao JL, Bernstein E, Celebi
894 JT, Chipuk JE. Activation of the Mitochondrial Fragmentation Protein DRP1 Correlates with
895 BRAF(V600E) Melanoma. J Invest Dermatol. 2015;135(10):2544-7. doi: 10.1038/jid.2015.196.
896 PubMed PMID: 26032958; PMCID: PMC4567922.
897 19. Frank S, Gaume B, Bergmann-Leitner ES, Leitner WW, Robert EG, Catez F, Smith CL,
898 Youle RJ. The role of dynamin-related protein 1, a mediator of mitochondrial fission, in
899 apoptosis. Dev Cell. 2001;1(4):515-25. Epub 2001/11/13. PubMed PMID: 11703942.
900 20. Thomas KJ, Jacobson MR. Defects in mitochondrial fission protein dynamin-related
901 protein 1 are linked to apoptotic resistance and autophagy in a lung cancer model. PloS one.
902 2012;7(9):e45319. Epub 2012/10/03. doi: 10.1371/journal.pone.0045319. PubMed PMID:
903 23028930; PMCID: 3447926.
904 21. Caino MC, Ghosh JC, Chae YC, Vaira V, Rivadeneira DB, Faversani A, Rampini P,
905 Kossenkov AV, Aird KM, Zhang R, Webster MR, Weeraratna AT, Bosari S, Languino LR, Altieri
906 DC. PI3K therapy reprograms mitochondrial trafficking to fuel tumor cell invasion. Proc Natl

907 Acad Sci U S A. 2015;112(28):8638-43. doi: 10.1073/pnas.1500722112. PubMed PMID:
908 26124089; PMCID: PMC4507184.
909 22. Farrand L, Kim JY, Im-Aram A, Suh JY, Lee HJ, Tsang BK. An improved quantitative
910 approach for the assessment of mitochondrial fragmentation in chemoresistant ovarian cancer
911 cells. PLoS One. 2013;8(9):e74008. Epub 2013/09/09. doi: 10.1371/journal.pone.0074008.
912 PubMed PMID: 24040144; PMCID: PMC3767598.
913 23. Kong B, Wang Q, Fung E, Xue K, Tsang BK. p53 is required for cisplatin-induced
914 processing of the mitochondrial fusion protein L-Opa1 that is mediated by the mitochondrial
915 metallopeptidase Oma1 in gynecologic cancers. The Journal of biological chemistry.
916 2014;289(39):27134-45. doi: 10.1074/jbc.M114.594812. PubMed PMID: 25112877; PMCID:
917 PMC4175349.
918 24. Macdonald PJ, Francy CA, Stepanyants N, Lehman L, Baglio A, Mears JA, Qi X,
919 Ramachandran R. Distinct Splice Variants of Dynamin-related Protein 1 Differentially Utilize
920 Mitochondrial Fission Factor as an Effector of Cooperative GTPase Activity. J Biol Chem.
921 2016;291(1):493-507. Epub 2015/11/19. doi: 10.1074/jbc.M115.680181. PubMed PMID:
922 26578513; PMCID: PMC4697187.
923 25. Rosdah AA, Smiles WJ, Oakhill JS, Scott JW, Langendorf CG, Delbridge LMD, Holien
924 JK, Lim SY. New perspectives on the role of Drp1 isoforms in regulating mitochondrial
925 pathophysiology. Pharmacol Ther. 2020;213:107594. Epub 2020/06/01. doi:
926 10.1016/j.pharmthera.2020.107594. PubMed PMID: 32473962.
927 26. Itoh K, Adachi Y, Yamada T, Suzuki TL, Otomo T, McBride HM, Yoshimori T, Iijima M,
928 Sesaki H. A brain-enriched Drp1 isoform associates with lysosomes, late endosomes, and the
929 plasma membrane. J Biol Chem. 2018;293(30):11809-22. Epub 2018/06/02. doi:
930 10.1074/jbc.RA117.001253. PubMed PMID: 29853636; PMCID: PMC6066318.
931 27. Strack S, Wilson TJ, Cribbs JT. Cyclin-dependent kinases regulate splice-specific
932 targeting of dynamin-related protein 1 to microtubules. J Cell Biol. 2013;201(7):1037-51. doi:
933 10.1083/jcb.201210045. PubMed PMID: 23798729; PMCID: PMC3691453.
934 28. Howng SL, Sy WD, Cheng TS, Lieu AS, Wang C, Tzou WS, Cho CL, Hong YR.
935 Genomic organization, alternative splicing, and promoter analysis of human dynamin-like
936 protein gene. Biochem Biophys Res Commun. 2004;314(3):766-72. Epub 2004/01/27. doi:
937 10.1016/j.bbrc.2003.12.172. PubMed PMID: 14741701.
938 29. Chen CH, Howng SL, Hwang SL, Chou CK, Liao CH, Hong YR. Differential expression
939 of four human dynamin-like protein variants in brain tumors. DNA Cell Biol. 2000;19(3):189-94.
940 Epub 2000/04/05. doi: 10.1089/104454900314573. PubMed PMID: 10749171.

941 30. Dier U, Shin DH, Hemachandra LP, Uusitalo LM, Hempel N. Bioenergetic analysis of
942 ovarian cancer cell lines: profiling of histological subtypes and identification of a mitochondria-
943 defective cell line. PLoS One. 2014;9(5):e98479. Epub 2014/05/27. doi:
944 10.1371/journal.pone.0098479. PubMed PMID: 24858344; PMCID: PMC4032324.
945 31. Tsuyoshi H, Orisaka M, Fujita Y, Asare-Werehene M, Tsang BK, Yoshida Y. Prognostic
946 impact of Dynamin related protein 1 (Drp1) in epithelial ovarian cancer. BMC Cancer.
947 2020;20(1):467. Epub 2020/05/26. doi: 10.1186/s12885-020-06965-4. PubMed PMID:
948 32448194; PMCID: PMC7247242.
949 32. Uo T, Dworzak J, Kinoshita C, Inman DM, Kinoshita Y, Horner PJ, Morrison RS. Drp1
950 levels constitutively regulate mitochondrial dynamics and cell survival in cortical neurons. Exp
951 Neurol. 2009;218(2):274-85. Epub 2009/05/19. doi: 10.1016/j.expneurol.2009.05.010. PubMed
952 PMID: 19445933; PMCID: PMC2733949.
953 33. Yoon Y, Pitts KR, Dahan S, McNiven MA. A novel dynamin-like protein associates with
954 cytoplasmic vesicles and tubules of the endoplasmic reticulum in mammalian cells. J Cell Biol.
955 1998;140(4):779-93. doi: 10.1083/jcb.140.4.779. PubMed PMID: 9472031; PMCID:
956 PMC2141745.
957 34. Michalska BM, Kwapiszewska K, Szczepanowska J, Kalwarczyk T, Patalas-Krawczyk P,
958 Szczepanski K, Holyst R, Duszynski J, Szymanski J. Insight into the fission mechanism by
959 quantitative characterization of Drp1 protein distribution in the living cell. Sci Rep.
960 2018;8(1):8122. Epub 2018/05/29. doi: 10.1038/s41598-018-26578-z. PubMed PMID:
961 29802333; PMCID: PMC5970238.
962 35. Li J, Huang Q, Long X, Guo X, Sun X, Jin X, Li Z, Ren T, Yuan P, Huang X, Zhang H,
963 Xing J. Mitochondrial elongation-mediated glucose metabolism reprogramming is essential for
964 tumour cell survival during energy stress. Oncogene. 2017;36(34):4901-12. Epub 2017/04/25.
965 doi: 10.1038/onc.2017.98. PubMed PMID: 28436948.
966 36. Skulachev VP. Mitochondrial filaments and clusters as intracellular power-transmitting
967 cables. Trends Biochem Sci. 2001;26(1):23-9. Epub 2001/02/13. doi: 10.1016/s0968-
968 0004(00)01735-7. PubMed PMID: 11165513.
969 37. Varanita T, Soriano ME, Romanello V, Zaglia T, Quintana-Cabrera R, Semenzato M,
970 Menabo R, Costa V, Civiletto G, Pesce P, Viscomi C, Zeviani M, Di Lisa F, Mongillo M, Sandri
971 M, Scorrano L. The OPA1-dependent mitochondrial cristae remodeling pathway controls
972 atrophic, apoptotic, and ischemic tissue damage. Cell Metab. 2015;21(6):834-44. Epub
973 2015/06/04. doi: 10.1016/j.cmet.2015.05.007. PubMed PMID: 26039448; PMCID:
974 PMC4457892.

975 38. Cogliati S, Frezza C, Soriano ME, Varanita T, Quintana-Cabrera R, Corrado M, Cipolat
976 S, Costa V, Casarin A, Gomes LC, Perales-Clemente E, Salviati L, Fernandez-Silva P, Enriquez
977 JA, Scorrano L. Mitochondrial cristae shape determines respiratory chain supercomplexes
978 assembly and respiratory efficiency. Cell. 2013;155(1):160-71. Epub 2013/09/24. doi:
979 10.1016/j.cell.2013.08.032. PubMed PMID: 24055366; PMCID: PMC3790458.
980 39. Cogliati S, Enriquez JA, Scorrano L. Mitochondrial Cristae: Where Beauty Meets
981 Functionality. Trends Biochem Sci. 2016;41(3):261-73. Epub 2016/02/10. doi:
982 10.1016/j.tibs.2016.01.001. PubMed PMID: 26857402.
983 40. Karbowski M, Lee YJ, Gaume B, Jeong SY, Frank S, Nechushtan A, Santel A, Fuller M,
984 Smith CL, Youle RJ. Spatial and temporal association of Bax with mitochondrial fission sites,
985 Drp1, and Mfn2 during apoptosis. J Cell Biol. 2002;159(6):931-8. Epub 2002/12/25. doi:
986 10.1083/jcb.200209124. PubMed PMID: 12499352; PMCID: PMC2173996.
987 41. Fonseca TB, Sanchez-Guerrero A, Milosevic I, Raimundo N. Mitochondrial fission
988 requires DRP1 but not dynamins. Nature. 2019;570(7761):E34-E42. Epub 2019/06/21. doi:
989 10.1038/s41586-019-1296-y. PubMed PMID: 31217603.
990 42. Otera H, Wang C, Cleland MM, Setoguchi K, Yokota S, Youle RJ, Mihara K. Mff is an
991 essential factor for mitochondrial recruitment of Drp1 during mitochondrial fission in mammalian
992 cells. J Cell Biol. 2010;191(6):1141-58. Epub 2010/12/15. doi: 10.1083/jcb.201007152. PubMed
993 PMID: 21149567; PMCID: PMC3002033.
994 43. Mopert K, Hajek P, Frank S, Chen C, Kaufmann J, Santel A. Loss of Drp1 function alters
995 OPA1 processing and changes mitochondrial membrane organization. Exp Cell Res.
996 2009;315(13):2165-80. Epub 2009/05/05. doi: 10.1016/j.yexcr.2009.04.016. PubMed PMID:
997 19409380.
998 44. Lima AR, Santos L, Correia M, Soares P, Sobrinho-Simoes M, Melo M, Maximo V.
999 Dynamin-Related Protein 1 at the Crossroads of Cancer. Genes (Basel). 2018;9(2). Epub
1000 2018/02/22. doi: 10.3390/genes9020115. PubMed PMID: 29466320; PMCID: PMC5852611.
1001 45. Banerjee R, Mukherjee A, Nagotu S. Mitochondrial dynamics and its impact on human
1002 health and diseases: inside the DRP1 blackbox. J Mol Med (Berl). 2022;100(1):1-21. Epub
1003 2021/10/18. doi: 10.1007/s00109-021-02150-7. PubMed PMID: 34657190.
1004 46. Xie Q, Wu Q, Horbinski CM, Flavahan WA, Yang K, Zhou W, Dombrowski SM, Huang Z,
1005 Fang X, Shi Y, Ferguson AN, Kashatus DF, Bao S, Rich JN. Mitochondrial control by DRP1 in
1006 brain tumor initiating cells. Nat Neurosci. 2015;18(4):501-10. Epub 2015/03/03. doi:
1007 10.1038/nn.3960. PubMed PMID: 25730670; PMCID: PMC4376639.

1008 47. Ciesla M, Ngoc PCT, Cordero E, Martinez AS, Morsing M, Muthukumar S, Beneventi G,
1009 Madej M, Munita R, Jonsson T, Lovgren K, Ebbesson A, Nodin B, Hedenfalk I, Jirstrom K,
1010 Vallon-Christersson J, Honeth G, Staaf J, Incarnato D, Pietras K, Bosch A, Bellodi C. Oncogenic
1011 translation directs spliceosome dynamics revealing an integral role for SF3A3 in breast cancer.
1012 Mol Cell. 2021;81(7):1453-68 e12. Epub 2021/03/05. doi: 10.1016/j.molcel.2021.01.034.
1013 PubMed PMID: 33662273.
1014 48. Gao T, Zhang X, Zhao J, Zhou F, Wang Y, Zhao Z, Xing J, Chen B, Li J, Liu S. SIK2
1015 promotes reprogramming of glucose metabolism through PI3K/AKT/HIF-1alpha pathway and
1016 Drp1-mediated mitochondrial fission in ovarian cancer. Cancer Lett. 2020;469:89-101. Epub
1017 2019/10/23. doi: 10.1016/j.canlet.2019.10.029. PubMed PMID: 31639424.
1018 49. van der Bliek AM. Fussy mitochondria fuse in response to stress. EMBO J.
1019 2009;28(11):1533-4. Epub 2009/06/06. doi: 10.1038/emboj.2009.130. PubMed PMID:
1020 19494844; PMCID: PMC2693156.
1021 50. Tondera D, Grandemange S, Jourdain A, Karbowski M, Mattenberger Y, Herzig S, Da
1022 Cruz S, Clerc P, Raschke I, Merkwirth C, Ehses S, Krause F, Chan DC, Alexander C, Bauer C,
1023 Youle R, Langer T, Martinou JC. SLP-2 is required for stress-induced mitochondrial hyperfusion.
1024 EMBO J. 2009;28(11):1589-600. Epub 2009/04/11. doi: 10.1038/emboj.2009.89. PubMed
1025 PMID: 19360003; PMCID: PMC2693158.
1026 51. Grieco JP, Allen ME, Perry JB, Wang Y, Song Y, Rohani A, Compton SLE, Smyth JW,
1027 Swami NS, Brown DA, Schmelz EM. Progression-Mediated Changes in Mitochondrial
1028 Morphology Promotes Adaptation to Hypoxic Peritoneal Conditions in Serous Ovarian Cancer.
1029 Front Oncol. 2020;10:600113. Epub 2021/02/02. doi: 10.3389/fonc.2020.600113. PubMed
1030 PMID: 33520711; PMCID: PMC7838066.
1031 52. Anderson AS, Roberts PC, Frisard MI, Hulver MW, Schmelz EM. Ovarian tumor-initiating
1032 cells display a flexible metabolism. Exp Cell Res. 2014;328(1):44-57. Epub 2014/08/31. doi:
1033 10.1016/j.yexcr.2014.08.028. PubMed PMID: 25172556; PMCID: PMC4260041.
1034 53. Ngo J, Choi DW, Stanley IA, Stiles L, Molina AJA, Chen PH, Lako A, Sung ICH,
1035 Goswami R, Kim MY, Miller N, Baghdasarian S, Kim-Vasquez D, Jones AE, Roach B, Gutierrez
1036 V, Erion K, Divakaruni AS, Liesa M, Danial NN, Shirihai OS. Mitochondrial morphology controls
1037 fatty acid utilization by changing CPT1 sensitivity to malonyl-CoA. EMBO J.
1038 2023;42(11):e111901. Epub 2023/03/15. doi: 10.15252/embj.2022111901. PubMed PMID:
1039 36917141; PMCID: PMC10233380.

1040 54. Alan L, Scorrano L. Shaping fuel utilization by mitochondria. Curr Biol.
1041 2022;32(12):R618-R23. Epub 2022/06/22. doi: 10.1016/j.cub.2022.05.006. PubMed PMID:
1042 35728541.
1043 55. Liesa M, Shirihai OS. Mitochondrial dynamics in the regulation of nutrient utilization and
1044 energy expenditure. Cell Metab. 2013;17(4):491-506. Epub 2013/04/09. doi:
1045 10.1016/j.cmet.2013.03.002. PubMed PMID: 23562075; PMCID: PMC5967396.
1046 56. Dar S, Chhina J, Mert I, Chitale D, Buekers T, Kaur H, Giri S, Munkarah A, Rattan R.
1047 Bioenergetic Adaptations in Chemoresistant Ovarian Cancer Cells. Sci Rep. 2017;7(1):8760.
1048 Epub 2017/08/20. doi: 10.1038/s41598-017-09206-0. PubMed PMID: 28821788; PMCID:
1049 PMC5562731.
1050 57. Bellance N, Benard G, Furt F, Begueret H, Smolkova K, Passerieux E, Delage JP, Baste
1051 JM, Moreau P, Rossignol R. Bioenergetics of lung tumors: alteration of mitochondrial biogenesis
1052 and respiratory capacity. Int J Biochem Cell Biol. 2009;41(12):2566-77. Epub 2009/08/29. doi:
1053 10.1016/j.biocel.2009.08.012. PubMed PMID: 19712747.
1054 58. Ghoneum A, Gonzalez D, Abdulfattah AY, Said N. Metabolic Plasticity in Ovarian
1055 Cancer Stem Cells. Cancers (Basel). 2020;12(5). Epub 2020/05/21. doi:
1056 10.3390/cancers12051267. PubMed PMID: 32429566; PMCID: PMC7281273.
1057 59. Yang L, Moss T, Mangala LS, Marini J, Zhao H, Wahlig S, Armaiz-Pena G, Jiang D,
1058 Achreja A, Win J, Roopaimoole R, Rodriguez-Aguayo C, Mercado-Uribe I, Lopez-Berestein G,
1059 Liu J, Tsukamoto T, Sood AK, Ram PT, Nagrath D. Metabolic shifts toward glutamine regulate
1060 tumor growth, invasion and bioenergetics in ovarian cancer. Mol Syst Biol. 2014;10(5):728.
1061 Epub 2014/05/07. doi: 10.1002/msb.20134892. PubMed PMID: 24799285; PMCID:
1062 PMC4188042.
1063 60. Pasto A, Bellio C, Pilotto G, Ciminale V, Silic-Benussi M, Guzzo G, Rasola A, Frasson C,
1064 Nardo G, Zulato E, Nicoletto MO, Manicone M, Indraccolo S, Amadori A. Cancer stem cells from
1065 epithelial ovarian cancer patients privilege oxidative phosphorylation, and resist glucose
1066 deprivation. Oncotarget. 2014;5(12):4305-19. Epub 2014/06/21. doi: 10.18632/oncotarget.2010.
1067 PubMed PMID: 24946808; PMCID: PMC4147325.
1068 61. Denkert C, Budczies J, Kind T, Weichert W, Tablack P, Sehouli J, Niesporek S, Konsgen
1069 D, Dietel M, Fiehn O. Mass spectrometry-based metabolic profiling reveals different metabolite
1070 patterns in invasive ovarian carcinomas and ovarian borderline tumors. Cancer Res.
1071 2006;66(22):10795-804. Epub 2006/11/17. doi: 10.1158/0008-5472.CAN-06-0755. PubMed
1072 PMID: 17108116.

1073 62. Fong MY, McDunn J, Kakar SS. Identification of metabolites in the normal ovary and
1074 their transformation in primary and metastatic ovarian cancer. PLoS One. 2011;6(5):e19963.
1075 Epub 2011/06/01. doi: 10.1371/journal.pone.0019963. PubMed PMID: 21625518; PMCID:
1076 PMC3098284 preliminary analysis of the data and final editing of the manuscript. However, as
1077 part of the University of Louisville's contract with Metabolon, Inc., he does not have any financial
1078 benefit or retention of invention or ownership rights, patentable or not. This does not affect
1079 adherence to PLoS ONE policies on sharing data and material.
1080 63. Mitra K, Wunder C, Roysam B, Lin G, Lippincott-Schwartz J. A hyperfused mitochondrial
1081 state achieved at G1-S regulates cyclin E buildup and entry into S phase. Proc Natl Acad Sci U
1082 S A. 2009;106(29):11960-5. Epub 2009/07/21. doi: 10.1073/pnas.0904875106. PubMed PMID:
1083 19617534; PMCID: PMC2710990.
1084 64. Spurlock B, Parker D, Basu MK, Hjelmeland A, Gc S, Liu S, Siegal GP, Gunter A, Moran
1085 A, Mitra K. Fine-tuned repression of Drp1-driven mitochondrial fission primes a 'stem/progenitor-
1086 like state' to support neoplastic transformation. Elife. 2021;10. Epub 2021/09/22. doi:
1087 10.7554/eLife.68394. PubMed PMID: 34545812; PMCID: PMC8497058.
1088 65. Kong B, Wang Q, Fung E, Xue K, Tsang BK. p53 is required for cisplatin-induced
1089 processing of the mitochondrial fusion protein L-Opa1 that is mediated by the mitochondrial
1090 metallopeptidase Oma1 in gynecologic cancers. J Biol Chem. 2014;289(39):27134-45. Epub
1091 2014/08/13. doi: 10.1074/jbc.M114.594812. PubMed PMID: 25112877; PMCID: PMC4175349.
1092 66. Zou GP, Yu CX, Shi SL, Li QG, Wang XH, Qu XH, Yang ZJ, Yao WR, Yan DD, Jiang
1093 LP, Wan YY, Han XJ. Mitochondrial Dynamics Mediated by DRP1 and MFN2 Contributes to
1094 Cisplatin Chemoresistance in Human Ovarian Cancer SKOV3 cells. J Cancer.
1095 2021;12(24):7358-73. Epub 2022/01/11. doi: 10.7150/jca.61379. PubMed PMID: 35003356;
1096 PMCID: PMC8734405.
1097 67. Tien JF, Mazloomian A, Cheng SG, Hughes CS, Chow CCT, Canapi LT, Oloumi A,
1098 Trigo-Gonzalez G, Bashashati A, Xu J, Chang VC, Shah SP, Aparicio S, Morin GB. CDK12
1099 regulates alternative last exon mRNA splicing and promotes breast cancer cell invasion. Nucleic
1100 Acids Res. 2017;45(11):6698-716. Epub 2017/03/24. doi: 10.1093/nar/gkx187. PubMed PMID:
1101 28334900; PMCID: PMC5499812.
1102 68. Song X, Wan X, Huang T, Zeng C, Sastry N, Wu B, James CD, Horbinski C, Nakano I,
1103 Zhang W, Hu B, Cheng SY. SRSF3-Regulated RNA Alternative Splicing Promotes Glioblastoma
1104 Tumorigenicity by Affecting Multiple Cellular Processes. Cancer Res. 2019;79(20):5288-301.
1105 Epub 2019/08/30. doi: 10.1158/0008-5472.CAN-19-1504. PubMed PMID: 31462429; PMCID:
1106 PMC6801100.

1107 69. Zhu J, Chen Z, Yong L. Systematic profiling of alternative splicing signature reveals
1108 prognostic predictor for ovarian cancer. Gynecol Oncol. 2018;148(2):368-74. Epub 2017/11/27.
1109 doi: 10.1016/j.ygyno.2017.11.028. PubMed PMID: 29191436.
1110 70. He X, Arslan AD, Pool MD, Ho TT, Darcy KM, Coon JS, Beck WT. Knockdown of
1111 splicing factor SRp20 causes apoptosis in ovarian cancer cells and its expression is associated
1112 with malignancy of epithelial ovarian cancer. Oncogene. 2011;30(3):356-65. Epub 2010/09/22.
1113 doi: 10.1038/onc.2010.426. PubMed PMID: 20856201; PMCID: PMC3010329.
1114 71. Shepherd TG, Theriault BL, Campbell EJ, Nachtigal MW. Primary culture of ovarian
1115 surface epithelial cells and ascites-derived ovarian cancer cells from patients. Nat Protoc.
1116 2006;1(6):2643-9. doi: 10.1038/nprot.2006.328. PubMed PMID: 17406520.
1117 72. Li H, Handsaker B, Wysoker A, Fennell T, Ruan J, Homer N, Marth G, Abecasis G,
1118 Durbin R, Genome Project Data Processing S. The Sequence Alignment/Map format and
1119 SAMtools. Bioinformatics. 2009;25(16):2078-9. Epub 2009/06/10. doi:
1120 10.1093/bioinformatics/btp352. PubMed PMID: 19505943; PMCID: PMC2723002.
1121 73. Patro R, Duggal G, Love MI, Irizarry RA, Kingsford C. Salmon provides fast and bias-
1122 aware quantification of transcript expression. Nat Methods. 2017;14(4):417-9. Epub 2017/03/07.
1123 doi: 10.1038/nmeth.4197. PubMed PMID: 28263959; PMCID: PMC5600148.
1124 74. Lam J, Katti P, Biete M, Mungai M, AshShareef S, Neikirk K, Garza Lopez E, Vue Z,
1125 Christensen TA, Beasley HK, Rodman TA, Murray SA, Salisbury JL, Glancy B, Shao J, Pereira
1126 RO, Abel ED, Hinton A, Jr. A Universal Approach to Analyzing Transmission Electron
1127 Microscopy with ImageJ. Cells. 2021;10(9). Epub 2021/09/29. doi: 10.3390/cells10092177.
1128 PubMed PMID: 34571826; PMCID: PMC8465115.
1129 75. Javed Z, Worley BL, Stump C, Shimko SS, Crawford LC, Mythreye K, Hempel N.
1130 Optimization of Extracellular Flux Assay to Measure Respiration of Anchorage-independent
1131 Tumor Cell Spheroids. Bio Protoc. 2022;12(4):e4321. Epub 2022/03/29. doi:
1132 10.21769/BioProtoc.4321. PubMed PMID: 35340292; PMCID: PMC8899553.

1133

1134

# Figures

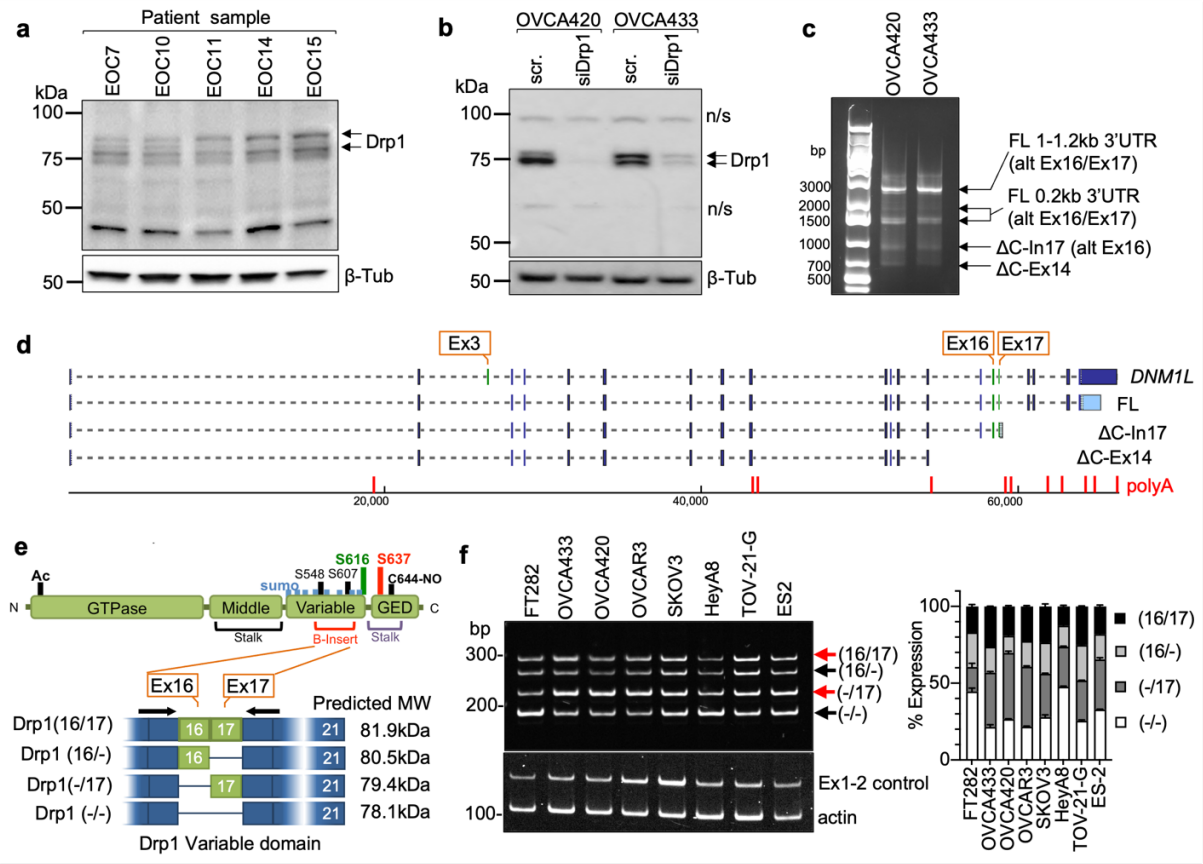


## Figure 1. Ovarian cancer cells express splice variants of Drp1/*DNM1L*.

a. Western blot analysis of Drp1 protein expression in patient ascites derived epithelial ovarian cancer cells (EOC), with the following histological classification: EOC7: HGSA stage IC; EOC10: granulosa tumor IV; EOC 11: carcinosarcoma stage IIIB; EOC14: HGSA stage IV; EOC15: HGSA stage IV. Arrows point to the predicted molecular weight protein (upper arrow) and a lower molecular weight band also prominently expressed.

b. Drp1 protein variants identified in OVCA420 and OVCA433 cells by western blotting using N-terminal anti-Drp1 monoclonal antibody ab184247. Specificity to Drp1 was assessed by siRNA mediated knock-down. Potential non-specific bands (n/s) are indicated. One representative blot from 3 independent replicates shown.

c. 3' RACE and subsequent sequencing of PCR products reveals that OVCA420 and OVCA433 cells express multiple *DNM1L* transcripts variants, including full length (FL) transcripts with alternatively spliced exons 16 and 17, and C terminal truncated transcripts at exon 14 (ΔC-Ex14) and intron 17 (ΔC-In17).

d. Schematic of transcript variants identified in OVCA420 and OVCA433 cells by 5' and 3' RACE (c), including alternate splicing of the variable domain exons 16 and 17 (panel c: alt Ex 16/17); variable lengths of 3'UTRs (panel c: FL 1-1.2kb, 0.2kb 3'UTR), and utilization of alternate proximal polyadenylation, resulting in two C terminal truncation variants, terminating in Intron 17 (ΔC-In17) and exon 14 (ΔC-Ex14). ΔC-In17 has two variants due to exon 16 alternate splicing and has a predicted STOP codon following a novel coding sequence for 16 amino acids within intron 17.

e. Schematic representation of the Drp1/*DNM1L* protein sequence functional domains and areas of post-translational modifications. The location of alternate spliced exons 16 and 17 is in the variable B-insert domain. Numbers in brackets of transcript names denote included exons in of the variable domain, dash denotes exon is spliced out.

f. RT-PCR with primers flanking the variable domain illustrates relative expression of the four *DNM1L* variable domain splice variants derived from alternate splicing of exons 16 and 17 in ovarian cancer cell lines (n=3, mean +/- SEM).

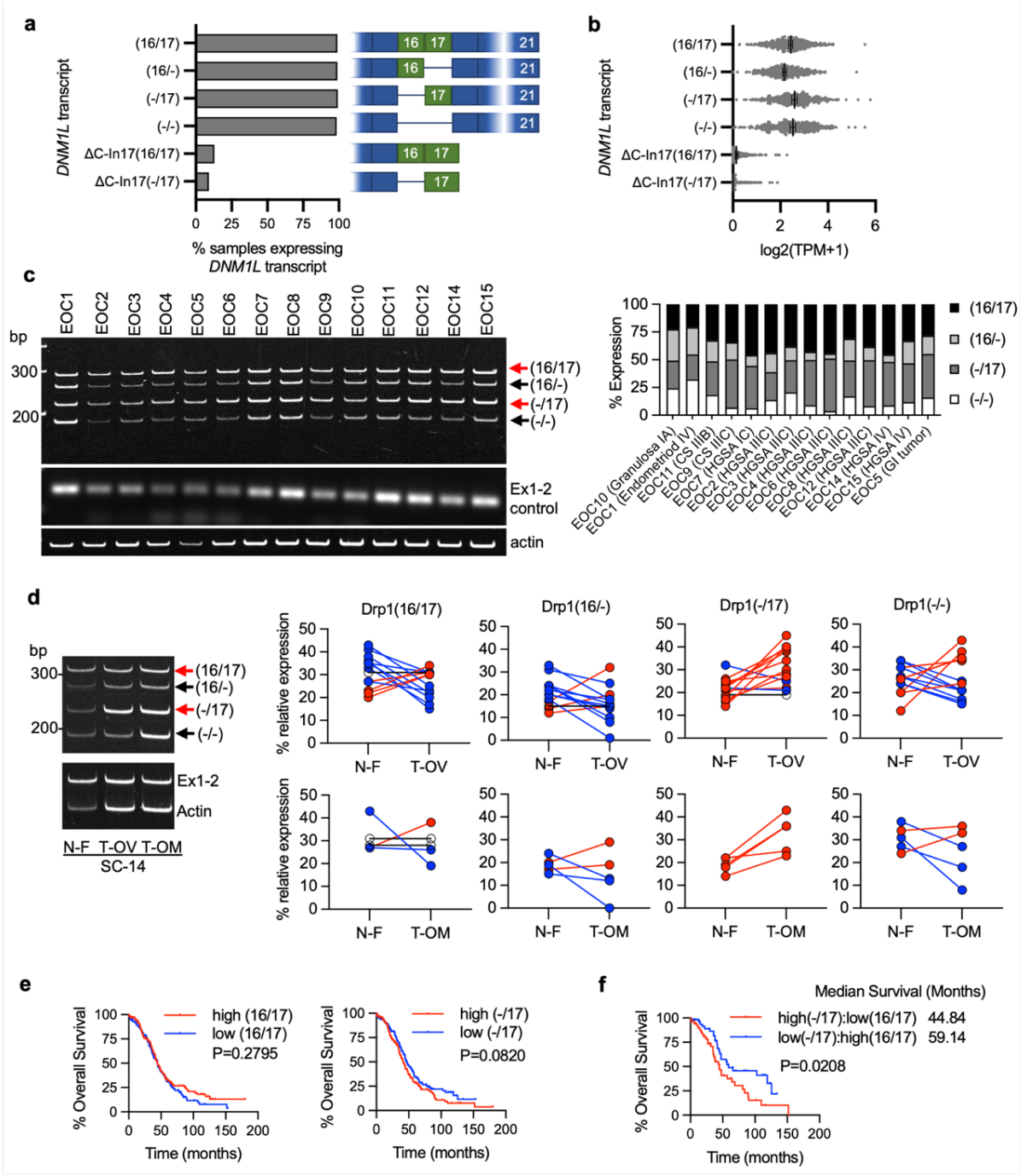


**Figure 2. Drp1/*DNM1L* transcript variant expression in ovarian cancer specimens.**

a. Frequency of Drp1/*DNM1L* transcript variant expression, focusing on full length variable domain (16/17) transcripts and C terminal truncation terminating in Intron 17 (ΔC-In17). Data represent percentage of specimens displaying TPM values >0.5 for each *DNM1L* transcript variant.

b. Expression levels of *DNM1L* transcript variants from TCGA data.

c. RT-PCR was used to show relative expression of DNM1L variable domain splice variants in a panel of patient ascites derived EOCs. Histologic classification and stage indicated in graph (right; CS: carcinosarcoma; HGSA: high grade serous adenocarcinoma; GI: gastrointestinal).

d. Representative RT-PCR (left) of *DNM1L* variable domain splice variant expression from normal fallopian tube (N-F), and matched ovarian (T-OV) and omental tumors (T-OM). The relative expression of splice variant transcript Drp1(-/17) is consistently higher in ovarian tumor and omental tumor compared to matched

1175 normal fallopian tube specimens (blots see Extended Data Fig. 3; blue lines indicate decreased expression,
1176 red lines indicate increased expression and black lines indicate no change in expression relative to matched
1177 normal fallopian tube tissue).
1178 e. Overall survival of TCGA patients based on DNM1L variant expression. Samples were split at median log2
1179 TPM into high (n=184) and low expression (n=184; log-rank Mantel-Cox test).
1180 **f.** Overall survival comparison between samples displaying mutually exclusive high Drp1(-/17)/low Drp1(16/17)
1181 (n=52) and low Drp1(-/17)/high Drp1(16/17) (n=52) expression (low and high cutoffs based on median log2
1182 TPM; log-rank Mantel-Cox test).

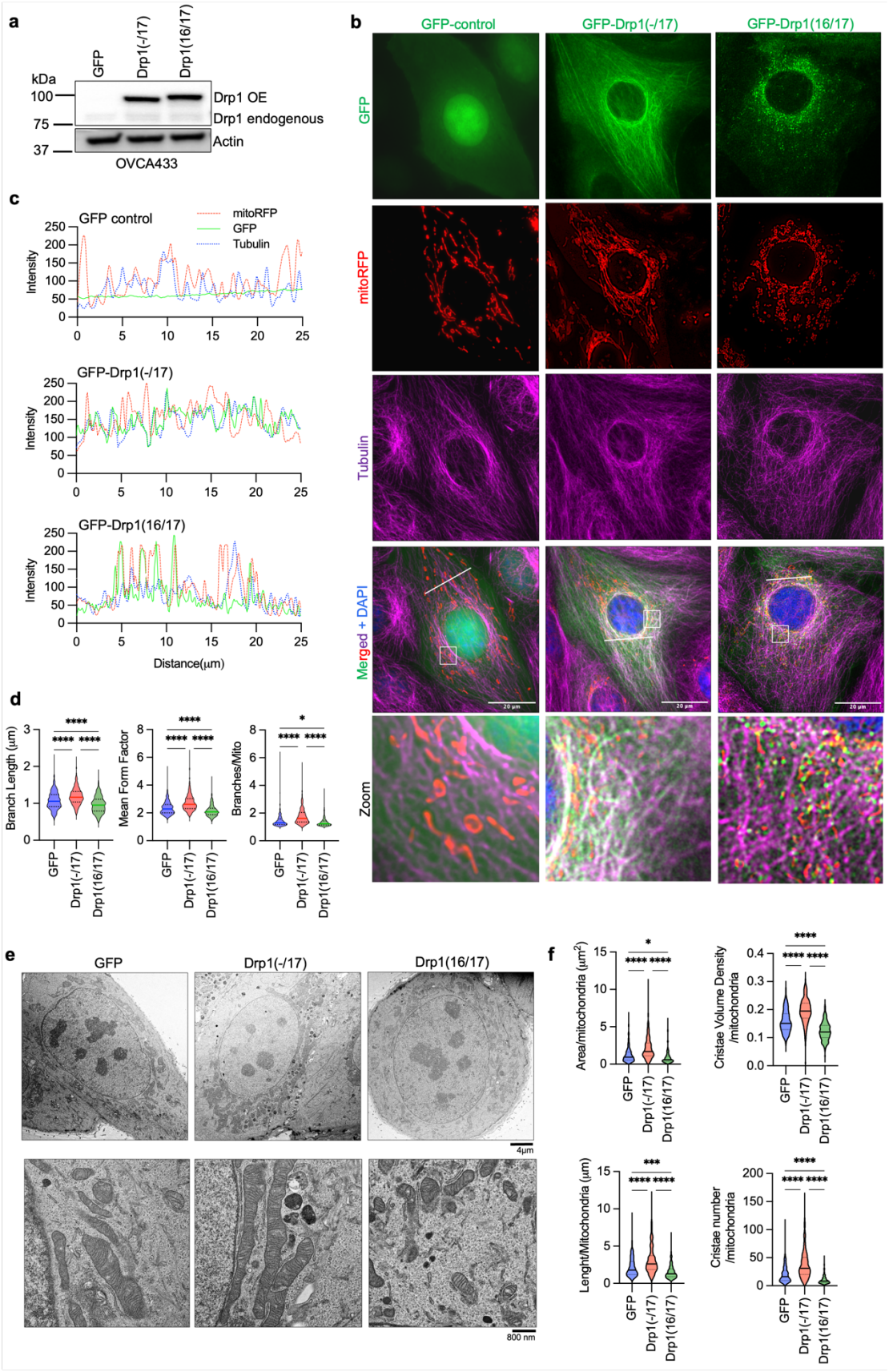
a
GFP
Drp1(-/17)
Drp1(16/17)
kDa
100
75
37
Drp1 OE
Drp1 endogenous
Actin
OVCA433
b
GFP-control
GFP-Drp1(-/17)
GFP-Drp1(16/17)
GFP
mitoRFP
Tubulin
Merged + DAPI
Zoom
c
GFP control
mitoRFP
GFP
Tubulin
Intensity
GFP-Drp1(-/17)
GFP-Drp1(16/17)
Distance(μm)
d
Branch Length (μm)
Mean Form Factor
Branches/Mito
GFP
Drp1(-/17)
Drp1(16/17)
e
GFP
Drp1(-/17)
Drp1(16/17)
4μm
800 nm
f
Area/mitochondria (μm²)
Cristae Volume Density /mitochondria
Lenght/Mitochondria (μm)
Cristae number /mitochondria

1183

**Figure 3. Drp1(-/17) displays decreased association with mitochondria, and its expression increases mitochondrial length and cristae density relative to Drp1(16/17).**

a. Western blot analysis following overexpression of GFP-tagged Drp1(-/17), Drp1(16/17) GFP vector control in OVCA433 cells.
b. Representative epifluorescence images of mitochondrial morphology and Drp1 distribution in OVCA433 cells. (Green: GFP or GFP-tagged Drp, Red: mito-RFP to label mitochondria, Magenta: Tubulin immunostained with anti-Tubulin antibody and Blue: DAPI). Drp1(-/17) shows a distinct pattern of co-localization with Tubulin, differing from the traditional punctate staining of Drp1 at mitochondria, a characteristic observed with Drp1(16/17). Scale bar: 20 µm.
c. Representative histograms of fluorescence intensity (white line in images on right) illustrate that Drp1(-/17) (green) is more closely aligned with Tubulin (blue) and less so with mitochondria (red), pointing towards reduced mitochondria association. In contrast, Drp1(16/17) peaks coincide with mitochondrial (red) peaks, reflective of Drp1 mitochondrial fission puncta.
d. Drp1(-/17) expressing cells show a decrease in fission, evidenced by the presence of a more elongated and branched network of mitochondria than in cells expressing Drp1(16/17). Quantification of mitochondrial morphological represented by three independent descriptors as analyzed by mitochondria analyzer in ImageJ. n = 498 cells from GFP-control, n = 568 cells from Drp1(-/17) and n=553 cells from Drp1(16/17) were analyzed. (one-way ANOVA Mean Form Factor $p < 0.0001$; Branch Length $p < 0.0001$ and Branches/mito $p<0.0001$. Tukey's post test *$p<0.05$, ****$p < 0.0001$).
e. Drp1(-/17) expressing cells have more fused mitochondria with greater cristae organization and volume. Representative Transmission EM images of OVCA433 cells. Arrows indicate the elongated mitochondria in Drp1(-1/7), fragmented mitochondria in Drp1(16/17) and a range of elongated to fragmented mitochondria in GFP cells. Scale bar: 4 µm and 800nm
f. Quantification of mitochondria and cristae from TEM images. magnification 800nM. n =156 cells from GFP-control, n =160 cells from Drp1(-/17) and n=157 cells from Drp1(16/17) were analyzed. (one-way ANOVA Area/mitochondria $p<0.0001$, Cristae volume density $p<0.0001$, Length/mitochondria $p<0.0001$ and Cristae number/mitochondria $p<0.0001$. Tukey's post test *$p < 0.05$, ***$p < 0.001$, ****$p < 0.0001$).

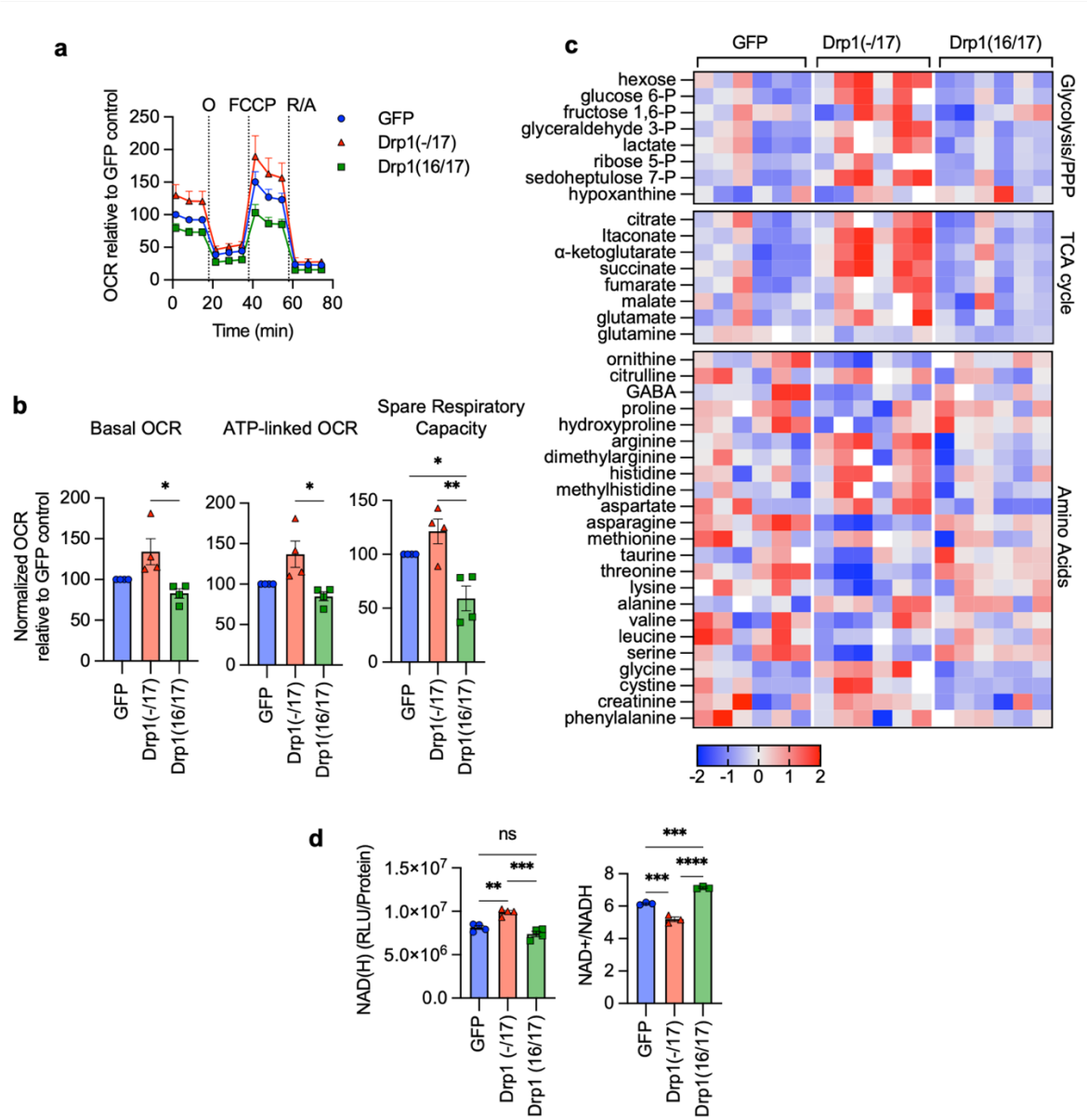


**Figure 4. Expression of Drp1(-/17) splice variant increases mitochondrial respiration and TCA cycle metabolites.**

a. Expression of Drp1(-/17) increases oxygen consumption rates (OCR) in OVCA433 cells as assessed by mitochondrial stress test using Seahorse extracellular flux analysis (O: oligomycin A, R/A: rotenone/antimycin A; OCR is normalized to cell viability and expressed relative to GFP control, n=4)
b. Basal OCR, ATP-linked OCR and spare respiratory capacity are increased in OVCA433 cells expressing Drp1(-/17) compared to Drp1(16/17). Data are expressed relative to GFP control (n=4, one-way ANOVA Basal OCR p=0.0144; ATP-linked OCR p=0.0131; spare respiratory capacity p=0.0034; Tukey's post test **p<0.01, ***p<0.001, ****p<0.0001)
c. Relative metabolite content of OVCA433 cells stably expressing GFP control, GFP-Drp1(-/17) or GFP-Drp1(16/17) as assessed by untargeted LC-HRMS (n=6, heatmap reflects z-scores of Area/iSTD values).
d. Total NAD(H) levels are increased in response to Drp1(-/17) expression relative to OVCA433 cells expressing GFP control or Drp1(16/17), while the ratio of NAD+/NADH is significantly decreased (one-way ANOVA NAD(H) n=4, p=0.0002; NAD+/NADH n=3 p<0.0001; Tukey's post test **p<0.01, ***p<0.001, ****p<0.0001).

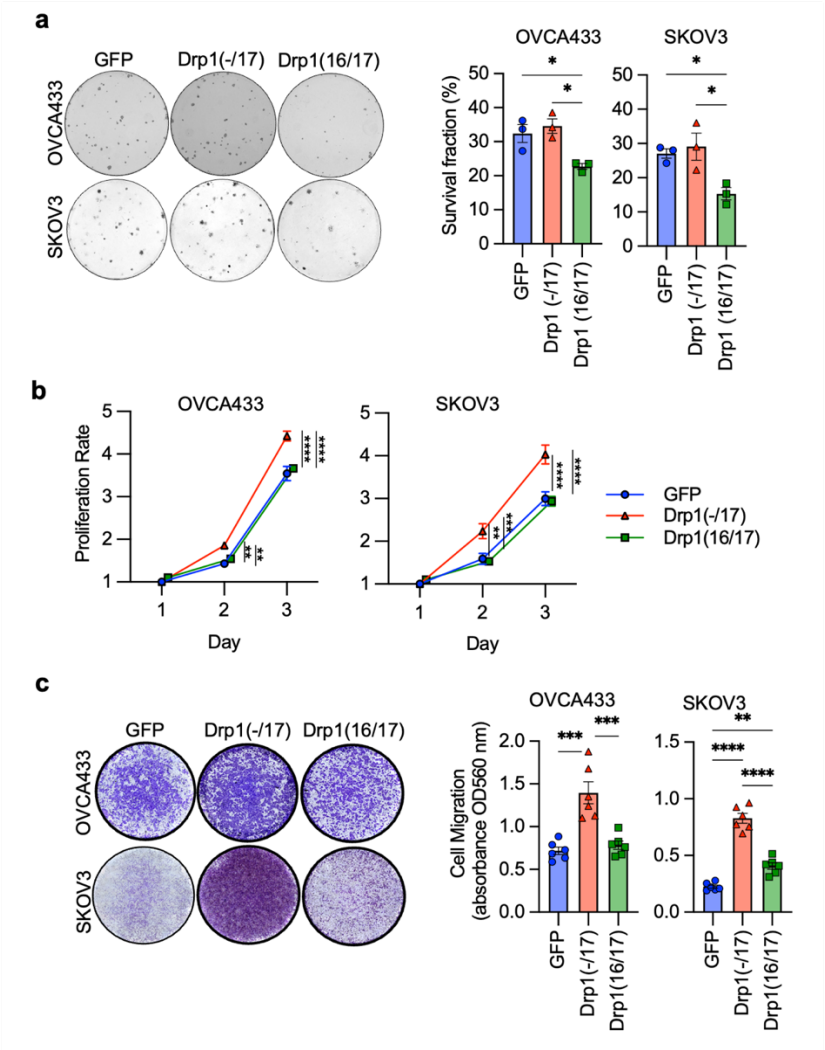


**Figure 5. Compared to Drp1(16/17), expression of Drp1(-/17) maintains clonogenic survival, promotes proliferation and migration of ovarian cancer cells.**

a. Drp1(16/17) expression lowers single cell clonogenic survival in both OVCA433 and SKOV3 cells. Cells (100/well) were seeded onto 6-well plates and stained with crystal violet after 7-10 days in culture. Colonies were quantified using ImageJ. Images are representative of 3 independent experiments (n=3, one-way ANOVA OVCA433 p=0.0128; SKOV3 p=0.0201. Tukey's post test *p<0.05).

b. Compared to Drp1(16/17) and GFP expression, Drp1(-/17) increases proliferation rate of OVCA433 and SKOV3 cells. Cell proliferation was assessed by FluoReporter dsDNA quantification and proliferation rate expressed as increase in the cell density relative to day 1 (n=3, two-way ANOVA group factor variance p<0.0001, Tukey's post test **p < 0.01, ***p < 0.001 and ****p < 0.0001).

c. Drp1 variants differently alter cell migration, with Drp1(-/17) expressing cells showing greater migratory ability than Drp1(16/17) or GFP control expressing cells. Cell migration was assessed using the Boyden chamber transwell assay and quantified by measuring the absorbance of the crystal violet staining of migrated cells. Images are representative of 3 independent assays (n=3, one-way ANOVA OVCA433 p=0.0155; SKOV3 p=0.0003. Tukey's post test *p<0.05, **p < 0.01. and ***p < 0.001).

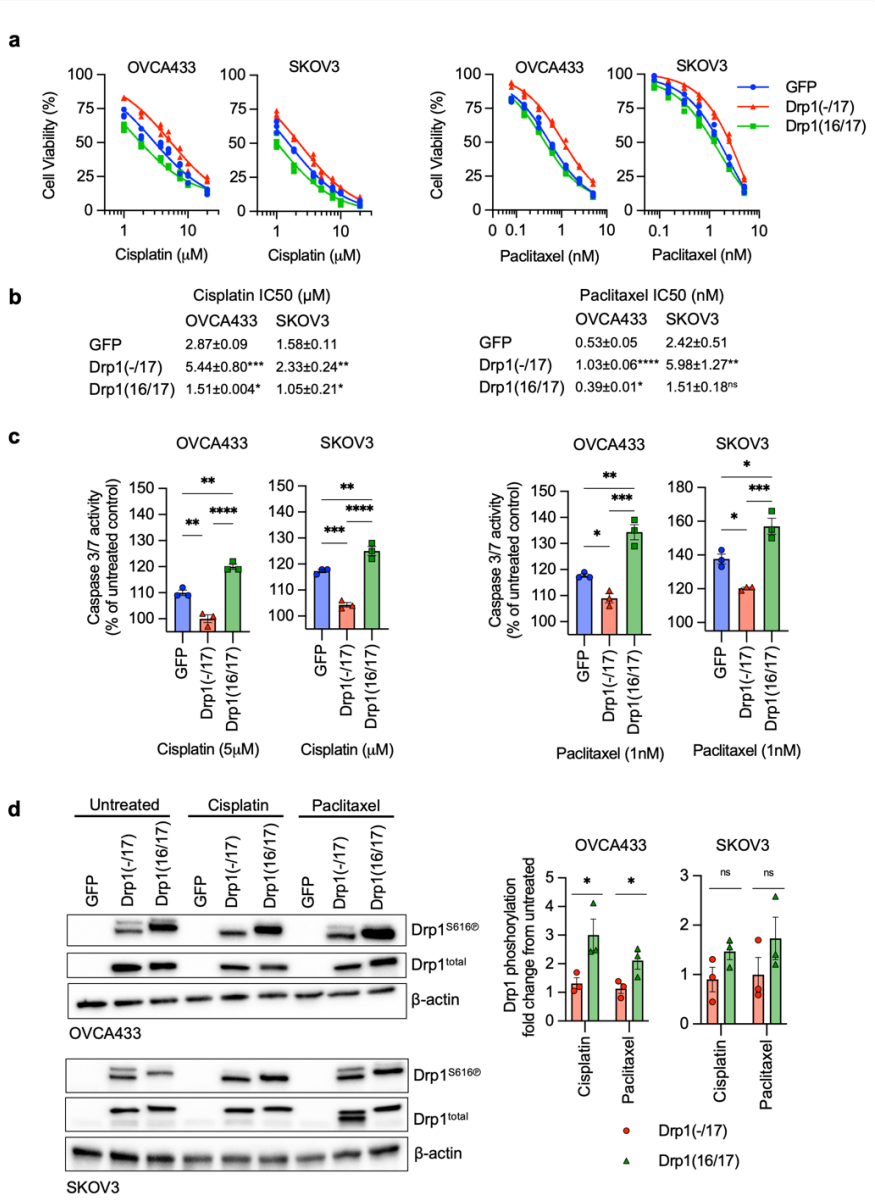


**Figure 6. Expression of Drp1(-/17) decreases sensitivity to chemotherapeutics.**

a. Dose response curves were derived from cell viability assays in response to cisplatin and paclitaxel treatment of OVCA433 and SKOV3 cells expressing GFP vector control, Drp1(-/17) and Drp1(16/17). Cells were plated into 96 wells and were exposed to increasing concentrations of cisplatin and paclitaxel for 72 hours respectively. Cell viability expressed as survival fraction was assessed by FluoReporter dsDNA quantification (n=3).

b. IC50 values were calculated from the above curves (n=3, one way ANOVA, Dunnet's post test comparison to GFP control *p<0.05, **p<0.01, ***p<0.001, ***p<0.0001).

c. Cells expressing Drp1(-/17) display abrogated apoptosis in response to cisplatin (5 μM) or paclitaxel (1 nM) treatment after 24 hours, as assessed using Caspase-Glo 3/7 assay (n=3, one-way ANOVA cisplatin OVCA433 p=<0.0001, SKOV3 p=<0.0001; paclitaxel OVCA433 p=0.0003, SKOV3 p=0.0006. Tukey's post test *p<0.05, **p<0.01, ***p<0.001, ****p<0.0001).

d. S616 phosphorylation of recombinant expressed Drp1 following cisplatin (5 μM) and paclitaxel (1 nM) treatment, as assessed by western blotting.

e. Change in Drp1 phosphorylation (S616) in response to cisplatin (5 μM) and paclitaxel (1 nM) is expressed relative to untreated control (Densitometry quantification was carried out using ImageJ and normalizing to total Drp1, n=3, unpaired t test *p<0.05).

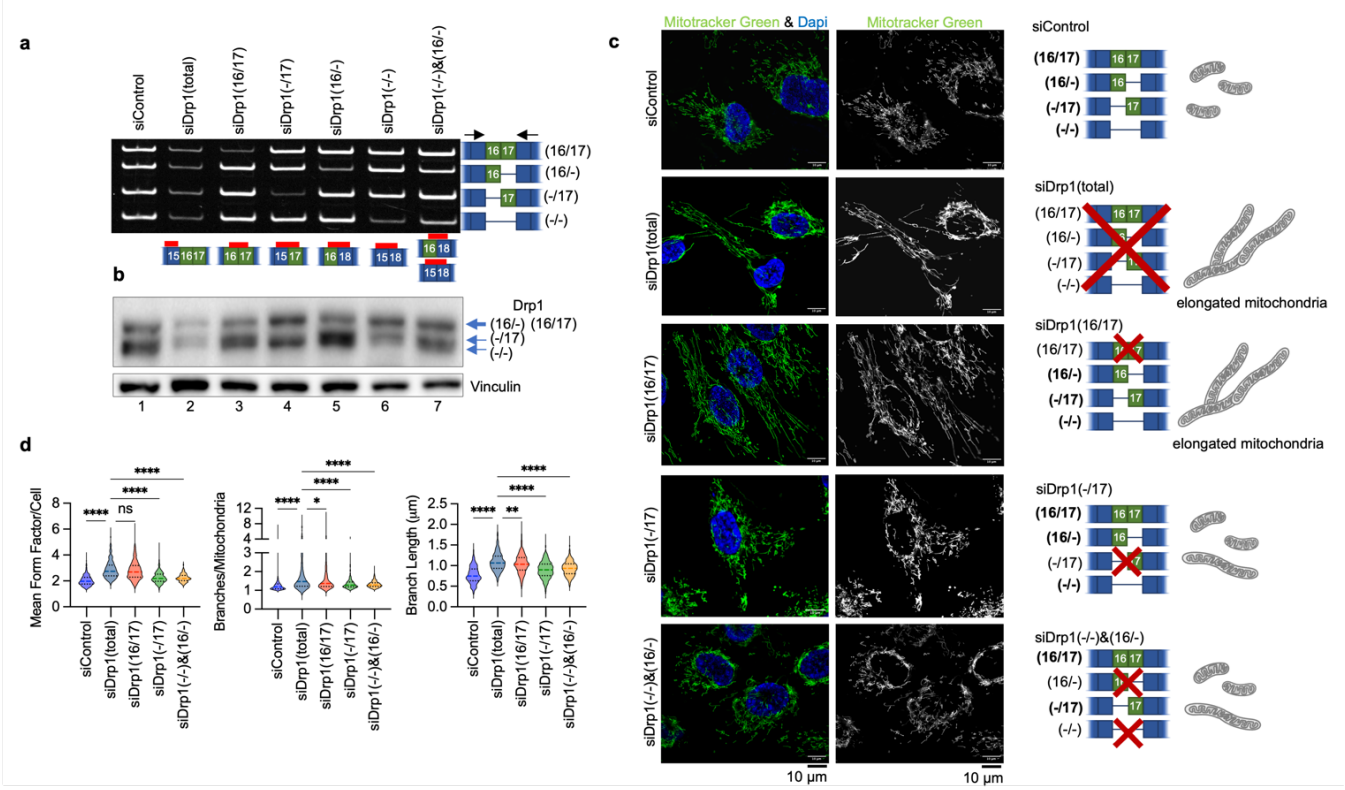


**Figure 7. Specific knock-down of endogenous Drp1 splice variants using siRNA and effects on mitochondrial morphology.**

a. RT-PCR demonstrating variant specific knock-down of Drp1 using splice variant specific siRNA in SKOV3 cells. One representative gel from independent replicates shown.
b. Splice variant specific siRNA mediated knock down of Drp1 protein in SKOV3 cells by western blotting. One representative blot from 3 independent replicates shown.
c. Representative epifluorescence images of mitochondrial morphology upon splice variant specific siRNA Drp1 knockdown in SKOV3 cells. (Green: mitotracker green and Blue: DAPI). The disruption of endogenous Drp1 splice variant expression differentially modifies mitochondrial dynamics. siDrp1(16/17) most closely replicates the elongated mitochondrial morphology observed following knock-down of all Drp1 variants (siDrp1 total), whereas siDrp1(-/17), and siDrp1(-/-)&(16/-) combination knock-down affect mitochondrial length and networking to a lesser degree. Scale bar: 10 µm.
d. Quantification of mitochondrial morphological represented by three independent descriptors as analyzed by mitochondria analyzer (ImageJ, analysis performed on sicontrol n = 560 cells, siDrp1(total) n = 334, siDrp1(16/17) n=630, siDrp1(-/17) n=655, siDrp1(-/-)&(16/-) n=555; one-way ANOVA Mean Form Factor $p < 0.0001$; Branch Length $p < 0.0001$ and Branches/mito $p<0.0001$. Tukey's post test was performed to assess differences between groups and comparisons of groups relative to siDrp1(total) are shown, *$p<0.05$, **$p<0.01$, ****$p < 0.0001$).

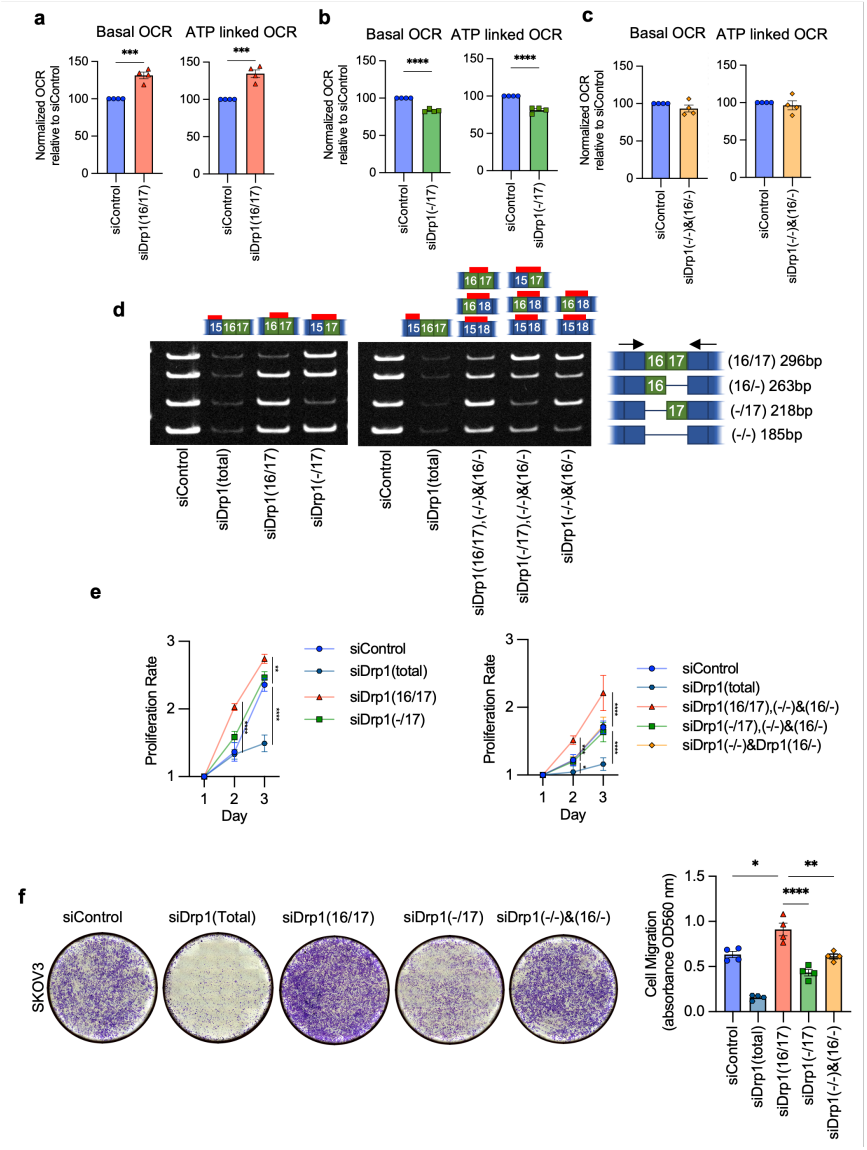


**Figure 8. Targeted knock-down of endogenous Drp1 splice variants in SKOV3 cells differentially affect mitochondrial respiration, proliferation and migration.**

a. Basal and ATP OCR indicating Mitochondrial respiration improved upon siRNA mediated knock down of the Drp1(16/17) splice variant, as assessed by mitochondrial stress test using Seahorse extracellular flux analysis (n=4, unpaired t-test. ***p<0.001).
b. Conversely, specific knock down of Drp1(-/17) decreased basal and ATP OCR indicating lower mitochondrial respiration (n=4, unpaired t-test. ****p<0.0001; OCR: oxygen consumption rate).
c. Mitochondrial respiration unchanged by combination Drp1(16/-) and (Drp1(-/) knock-down relative to siControl cells (n=4).
d. RT-PCR demonstrating knock-down of Drp1 using single splice variant specific siRNA or combination of splice variant specific siRNA enriching single Drp1 variant in cells to study cell proliferations changes with altered endogenous Drp1 variants. One representative gel from independent replicates shown.
e. Single variant knock-down of Drp1(16/17) and Drp1(-/17) variant enrichment with combination knock-down increases proliferation rate of SKOV3 cells relative to siControl. Cell proliferation was assessed by FluoReporter dsDNA quantification and proliferation rate expressed as increase in the cell density relative to day 1. (n=3, two-way ANOVA group factor variance p<0.0001, Tukey's post test was performed to assess

differences between groups and analysis comparing groups are shown, *p < 0.05, **p < 0.01, ***p < 0.001 and ****p < 0.0001).

f. Endogenous Drp1 splice variants differentially effect cell migration in SKOV3 cells, with siDrp1(16/17) increasing migratory ability while in contrast siDrp1(-/17) reduced cell migration than siControl cells. Post variant specific Drp1 knock-down, cell migration was assessed using the Boyden chamber transwell assay and quantified by measuring the absorbance of the crystal violet staining of migrated cells. Images are representative of 4 independent assays (n=4, one-way ANOVA ****p<0.0001. Tukey's post test was performed to assess differences between groups and analysis comparing siControl, siDrp1(16/17), siDrp1(-/17) and siDrp1(-/-)&(16/-) groups are shown, Tukey's multiple comparison *p<0.05, **p < 0.01. and ****p < 0.0001).

# Extended Data Figures

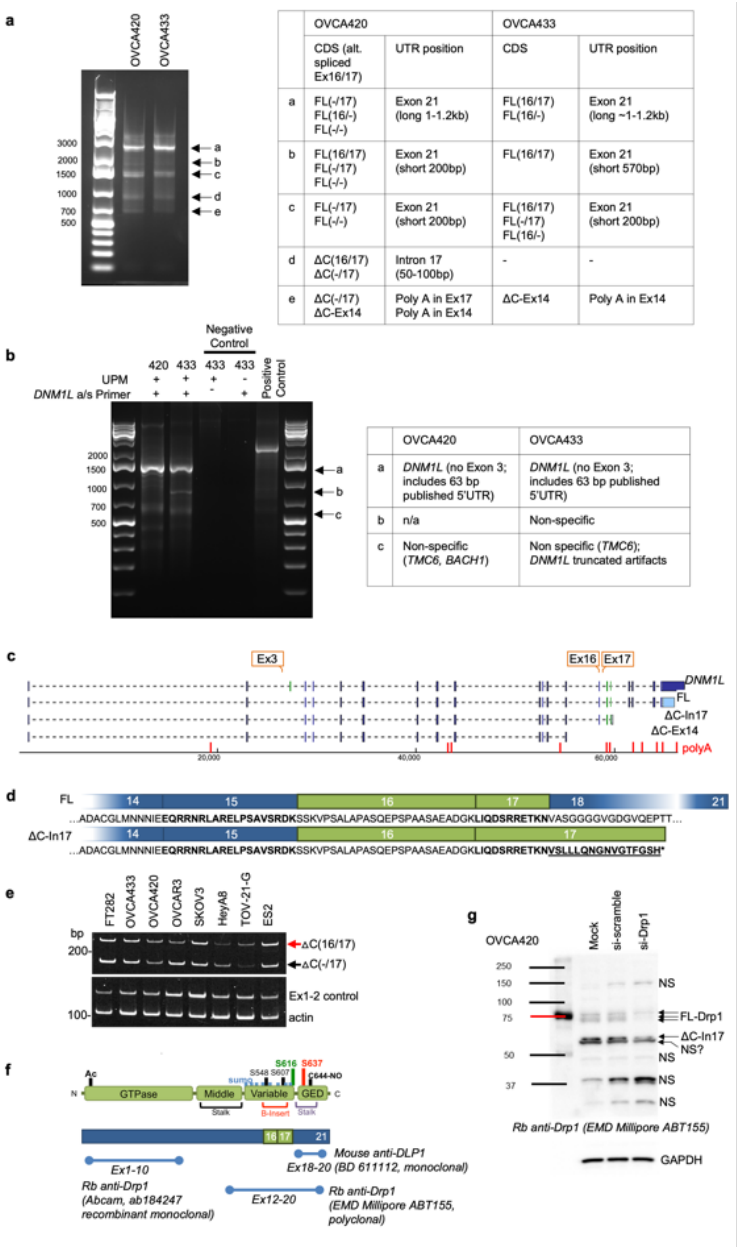


| | OVCA420 | | OVCA433 | |
|---|---|---|---|---|
| | CDS (alt. spliced Ex16/17) | UTR position | CDS | UTR position |
| a | FL(-/17)<br>FL(16/-)<br>FL(-/-) | Exon 21<br>(long 1-1.2kb) | FL(16/17)<br>FL(16/-) | Exon 21<br>(long ~1-1.2kb) |
| b | FL(16/17)<br>FL(-/17)<br>FL(-/-) | Exon 21<br>(short 200bp) | FL(16/17) | Exon 21<br>(short 570bp) |
| c | FL(-/17)<br>FL(-/-) | Exon 21<br>(short 200bp) | FL(16/17)<br>FL(-/17)<br>FL(16/-) | Exon 21<br>(short 200bp) |
| d | ΔC(16/17)<br>ΔC(-/17) | Intron 17<br>(50-100bp) | - | - |
| e | ΔC(-/17)<br>ΔC-Ex14 | Poly A in Ex17<br>Poly A in Ex14 | ΔC-Ex14 | Poly A in Ex14 |

| | OVCA420 | OVCA433 |
|---|---|---|
| a | *DNM1L* (no Exon 3; includes 63 bp published 5'UTR) | *DNM1L* (no Exon 3; includes 63 bp published 5'UTR) |
| b | n/a | Non-specific |
| c | Non-specific (*TMC6, BACH1*) | Non specific (*TMC6*); *DNM1L* truncated artifacts |

**Extended Data Figure 1. Identification of Drp1 transcript variants in ovarian cancer cell lines.**

a. 3' RACE reveals that ovarian cancer cell lines OVCA420 and OVCA433 express multiple Drp1/*DNM1L* transcripts variants, including full length (FL) transcripts with alternatively spliced exons 16 and 17, and C terminal truncated transcripts at exon 14 (ΔC-Ex14) and intron 17 (ΔC-In17). 3' RACE was carried out using SMARTer 3'5'RACE kit (Takara). PCR products from each cell line (a-e) were gel-extracted and cloned into the in-Fusion pRACE vector. 3-5 colonies per clone were selected for sequencing to determine the major5'RACE products in OVCA420 and OVCA433 cells (Table).

b. 5' RACE reveals that *DNM1L* transcripts expressed in OVCA420 and OVCA433 cell share the same 5'UTR and lack exon 3. 5' RACE was carried out using SMARTer 3'RACE kit (Takara) the with the Universal Primer A Mix (UPM) and the *DNM1L* specific antisense primer, positioned in Exon 12. PCR products from each cell line (a-c) were gel-extracted and cloned into the in-Fusion pRACE vector. 3-5 colonies per clone

1325 were selected for sequencing to determine the major 5'RACE products in OVCA420 and OVCA433 cells
1326 (Table).
1327 c. Transcript variants identified in OVCA420 and OVCA433 cells include alternate splicing of the variable
1328 domain exons 16 and 17; variable lengths of 3'UTRs, and utilization of proximal polyadenylation, resulting in
1329 two C terminal truncation variants, terminating in Intron 17 (ΔC-In17) and exon 14 (ΔC-Ex14; indicated in
1330 red; PolyA_DB v.3.2; PolyASites). 5'RACE demonstrated that ovarian cancer cell lines cell share the same
1331 5'UTR and lack exon 3.
1332 d. Schematic of the *DNM1L* variable domain Exons 16 and 17 alternatively spliced in ovarian cancer cells and
1333 corresponding amino acid sequences. The variant terminating in Intron 17 (ΔC-In17) also displays variable
1334 domain exon 16 alternate splicing and is predicted to encode an additional 16 amino acids from the adjacent
1335 intron to terminate at an alternate STOP codon.
1336 e. RT-PCR with primers designed to detect the intronic retention of the 3' region of ΔC-In17 illustrates that the
1337 *DNM1L* C terminal truncation variant terminating in Intron 17 can be detected in most ovarian cancer cell
1338 lines to variable degrees and that these transcripts can vary in their splicing of exon 16.
1339 f. Position of epitopes used to generate commercially available Drp1 antibodies. Note that C-terminal targeted
1340 antibody BD611112 is predicted not to recognize potential C-terminal truncations.
1341 g. Protein variants identified in the range of 65-80kDa by western are verified to be Drp1 by siRNA mediated
1342 knock-down. Non-specific bands (n/s) are not affected by siRNA against Drp1.

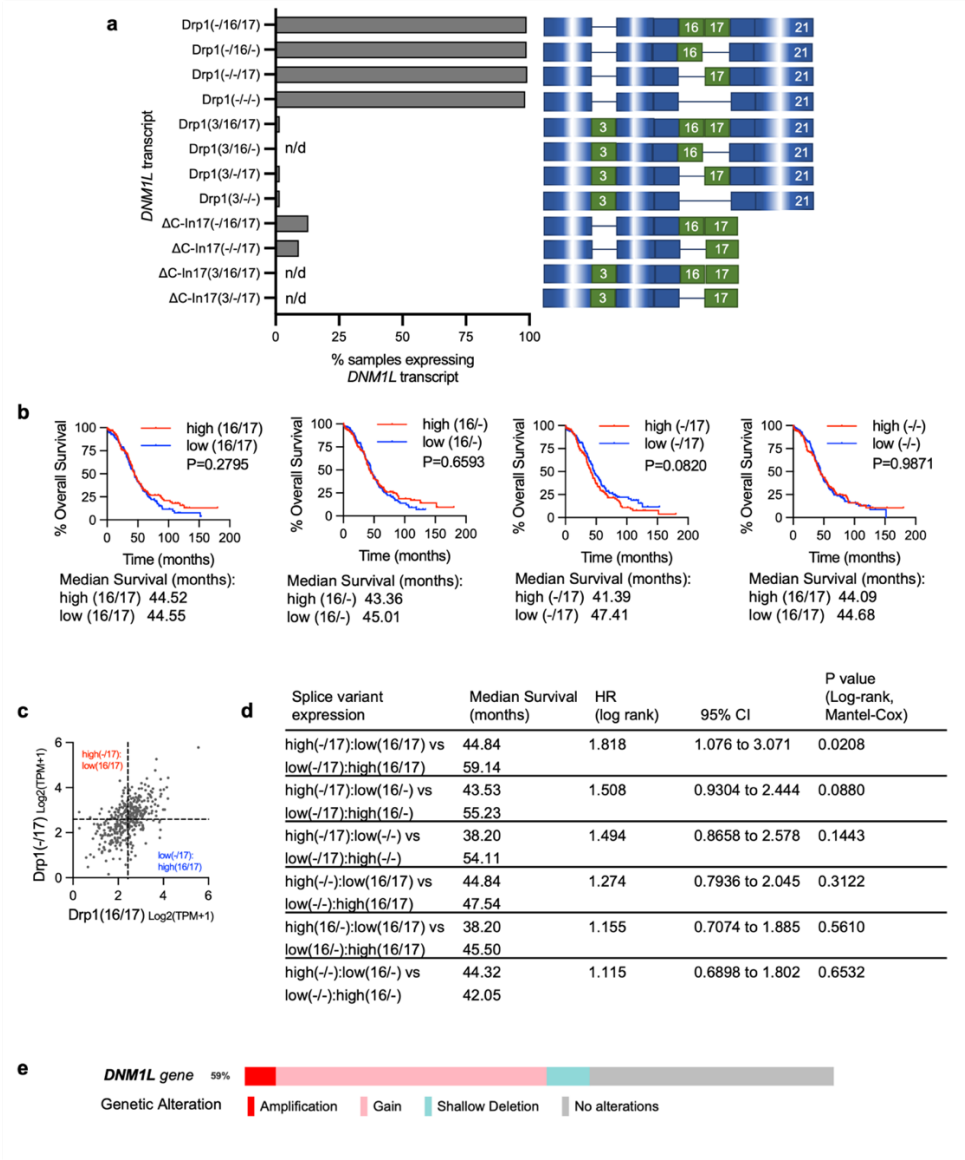


| Splice variant expression | Median Survival (months) | HR (log rank) | 95% CI | P value (Log-rank, Mantel-Cox) |
|---|---|---|---|---|
| high(-/17):low(16/17) vs low(-/17):high(16/17) | 44.84<br>59.14 | 1.818 | 1.076 to 3.071 | 0.0208 |
| high(-/17):low(16/-) vs low(-/17):high(16/-) | 43.53<br>55.23 | 1.508 | 0.9304 to 2.444 | 0.0880 |
| high(-/17):low(-/-) vs low(-/17):high(-/-) | 38.20<br>54.11 | 1.494 | 0.8658 to 2.578 | 0.1443 |
| high(-/-):low(16/17) vs low(-/-):high(16/17) | 44.84<br>47.54 | 1.274 | 0.7936 to 2.045 | 0.3122 |
| high(16/-):low(16/17) vs low(16/-):high(16/17) | 38.20<br>45.50 | 1.155 | 0.7074 to 1.885 | 0.5610 |
| high(-/-):low(16/-) vs low(-/-):high(16/-) | 44.32<br>42.05 | 1.115 | 0.6898 to 1.802 | 0.6532 |

**Extended Data Figure 2. Drp1/*DNM1L* transcript variant expression in ovarian cancer specimens from TCGA.**

a. Frequency of Drp1/*DNM1L* transcript variant expression, focusing on full length transcpri variants and alternatively spliced exons 3, 16 and 17 (3/16/17) transcripts and C terminal truncation terminating in Intron 17 (ΔC-In17). Dash denotes exon is spliced out. Data represent percentage of specimens displaying log2 TPM+1 values >0.5 for each DNM1L variant.
b. Overall survival of TCGA patients based on DNM1L variant expression. Samples were split at median log2 TPM into high (n=184) and low expression (n=184; log-rank Mantel-Cox test).
c. Drp1(-/17) expression relative to Drp1(16/17; log2 TPM+1). Mutually exclusive high and low expression of variant pairs is based on median log2 TPM+1 expression cut offs indicated by dotted line.
d. Overall survival data of TCGA ovarian cancer patients grouped into mutually exclusive high/low expression of Drp1 transcript variant pairs. Low and high cutoffs based on median expression. Patients with high Drp1(-/17) and low Drp1(16/17) expression display significantly decreased overall survival compared to patients with high Drp1(16/17) and low Drp1(-/17) transcript levels in their tumors.
e. *DNM1L* gene copy number alterations in 233 Ovarian Serous Cystadenocarcinoma cases with complete CNA data (TCGA, PanCancer Atlas). 5% of cases display high level amplification, 46% low level gain, and 7% shallow deletion.

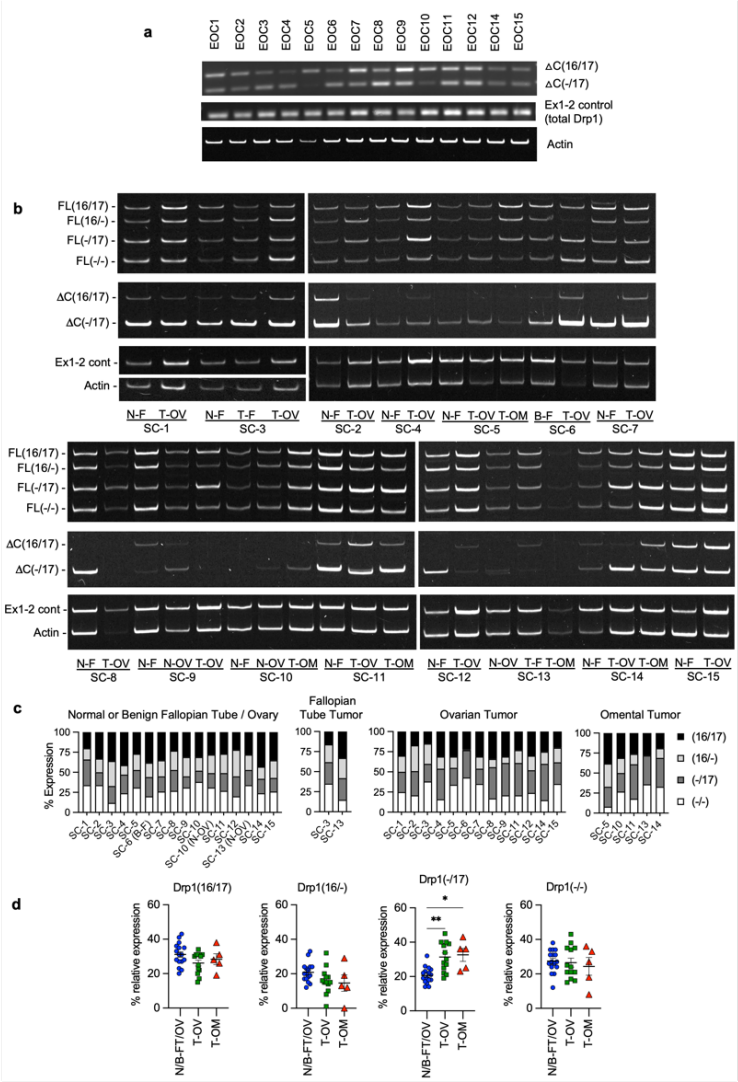


**Extended Data Figure 3.** ***Expression of DNM1L splice variants in matched patient specimens*****.**

a. RT-PCR was used to show relative expression of ΔC(-/17) and ΔC(16/17) truncated transcripts of DNM1L in a panel of patient ascites derived EOCs. (EOC9 & 11: carcinosarcoma; EOC 2,3,4 HGSA high grade serous adenocarcinoma; GI: gastrointestinal; tumor stage is indicated in Figure 2c).
b. RT-PCR of *DNM1L* variable domain splice variant expression from normal fallopian tube (N-F), and matched ovarian (T-OV) and omental tumors (T-OM). The relative expression of splice variant transcript Drp1(-/17) is consistently higher in ovarian tumor and omental tumor compared to matched normal fallopian tube specimens N=normal, T=tumor, B=benign, F=fallopian tube, OV= ovary, OM= omentum. All specimens were classified as HGSA, and the following stage: SC-1: IIIC, SC-2: IIIB, SC-3: IIIC, SC-4: IB, SC-5: IIIC, SC-6: IC3, SC-7: IIIB, SC-8: IIIC, SC-9: IVB, SC-10: IIIC, SC-11: IIIB, SC-12: IC2, SC-13: IIIC, SC-14: IIIC, SC-15: IIIB.
c. Quantification of relative Drp1 variable domain splice variant expression from panel b.
d. Comparison of relative expression of each variant between normal fallopian tube/ovary and ovarian tumor or omental tumor. Relative expression of Drp1(-/17) compared to other variants is significantly increased in ovarian tumors and omental tumors compared to matched normal tissues. (Mixed Effects Analysis with Tukey's post test. *$p<0.05$, **$p<0.01$).

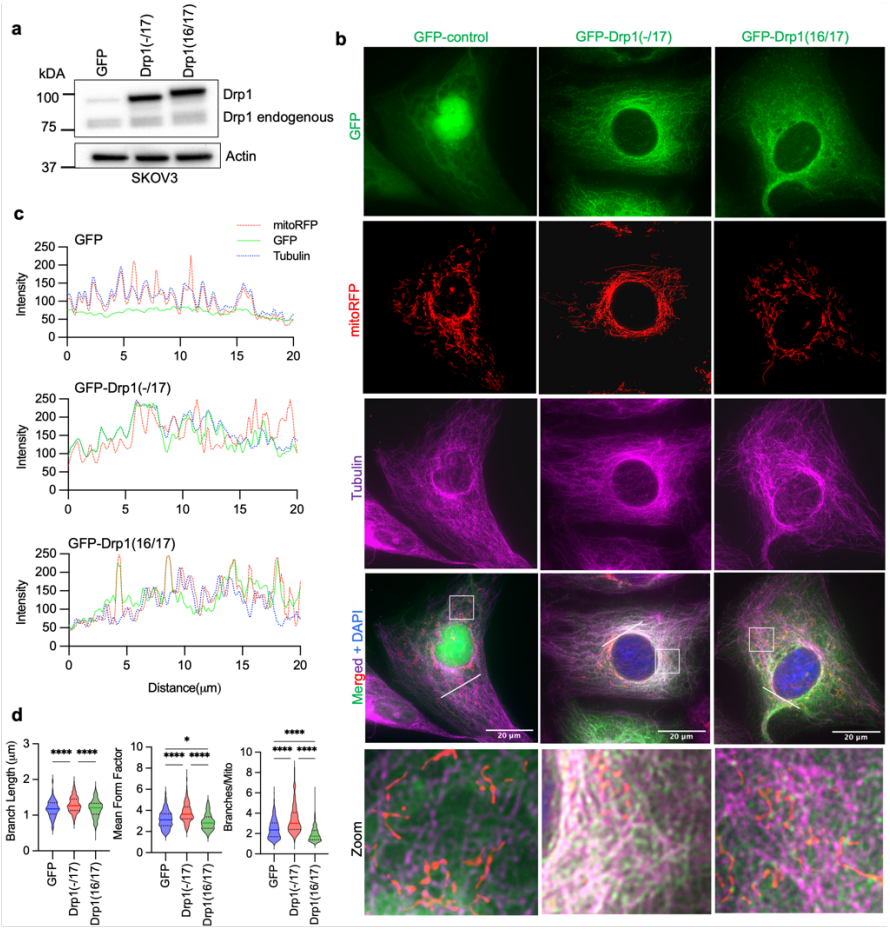


**Extended Data Figure 4: Drp1(-/17) displays decreased association with mitochondria and increased localization to microtubules in SKOV3 cells.**

a. Western blot analysis of GFP-tagged Drp1 protein expression in SKOV3 cells.
b. Representative epifluorescence images of mitochondrial morphology and Drp1 distribution in SKOV3 cells. (Green: GFP or GFP-tagged Drp, Red: mitochondria traced with mito-RFP, Magenta: Tubulin immunostained with anti-Tubulin antibody and Blue: DAPI). Drp1(-/17) expression in SKOV3 cells also shows a greater degree of co-localization with Tubulin as opposed to mitochondria, a contrast to the expression of Drp1(16/17), which exhibits the more traditional fission punctate staining at the mitochondria. Scale bar: 20 µm.
c. Representative histograms of fluorescence intensity (white line in images on right) illustrate that Drp1(-/17) (green) is more closely aligned with Tubulin (blue) and less so with mitochondria (red), pointing towards reduced mitochondria association. In contrast, Drp1(16/17) peaks coincide with mitochondrial (red) peaks, indicative of the Drp1 mitochondrial fission puncta.
d. Drp1(-/17) expression in SKOV3 exhibit diminished fission, as illustrated by their more elongated and interconnected mitochondrial network, in contrast to cells that express Drp1(16/17). Quantification of mitochondrial morphological represented by three independent descriptors as analyzed by mitochondria analyzer in ImageJ. n = 180 cells from GFP-control, n = 224 cells from Drp1(-/17) and n=252 cells from Drp1(16/17) were analyzed. (one-way ANOVA Mean Form Factor $p < 0.0001$; Branch Length $p < 0.0001$and Branches/mito $p < 0.0001$. Tukey's post test *$p<0.05$, ****$p < 0.0001$).

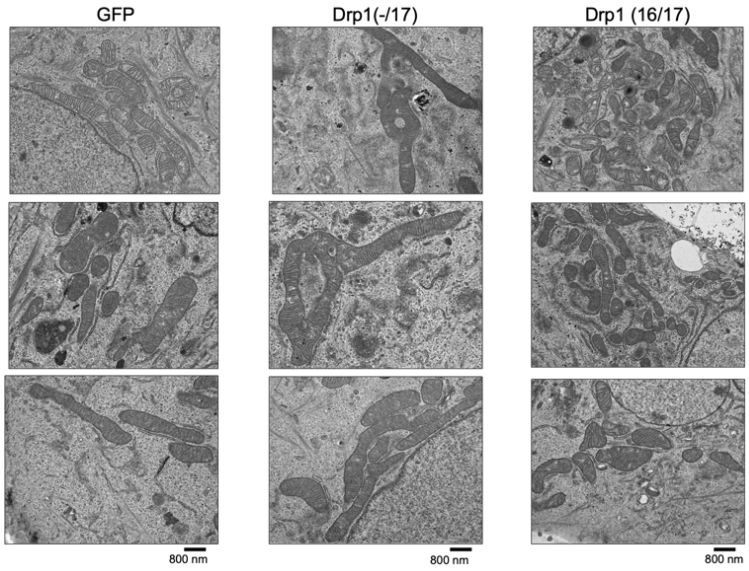


**Extended Data Figure 5: Drp1(-17) and Drp1(16/17) expression differentially alter mitochondrial architecture of OVCA433 cells.**
Representative TEM images from 3 individual biological replicates demonstrate a more fused mitochondrial morphology in Drp1(-/17) cells compared to the smaller, fragmented mitochondria characteristic of Drp1(16/17) cells. Meanwhile, mitochondria in GFP control cells exhibit a variety of forms, from elongated to smaller, fragmented shapes. Scale bar: 800nm.

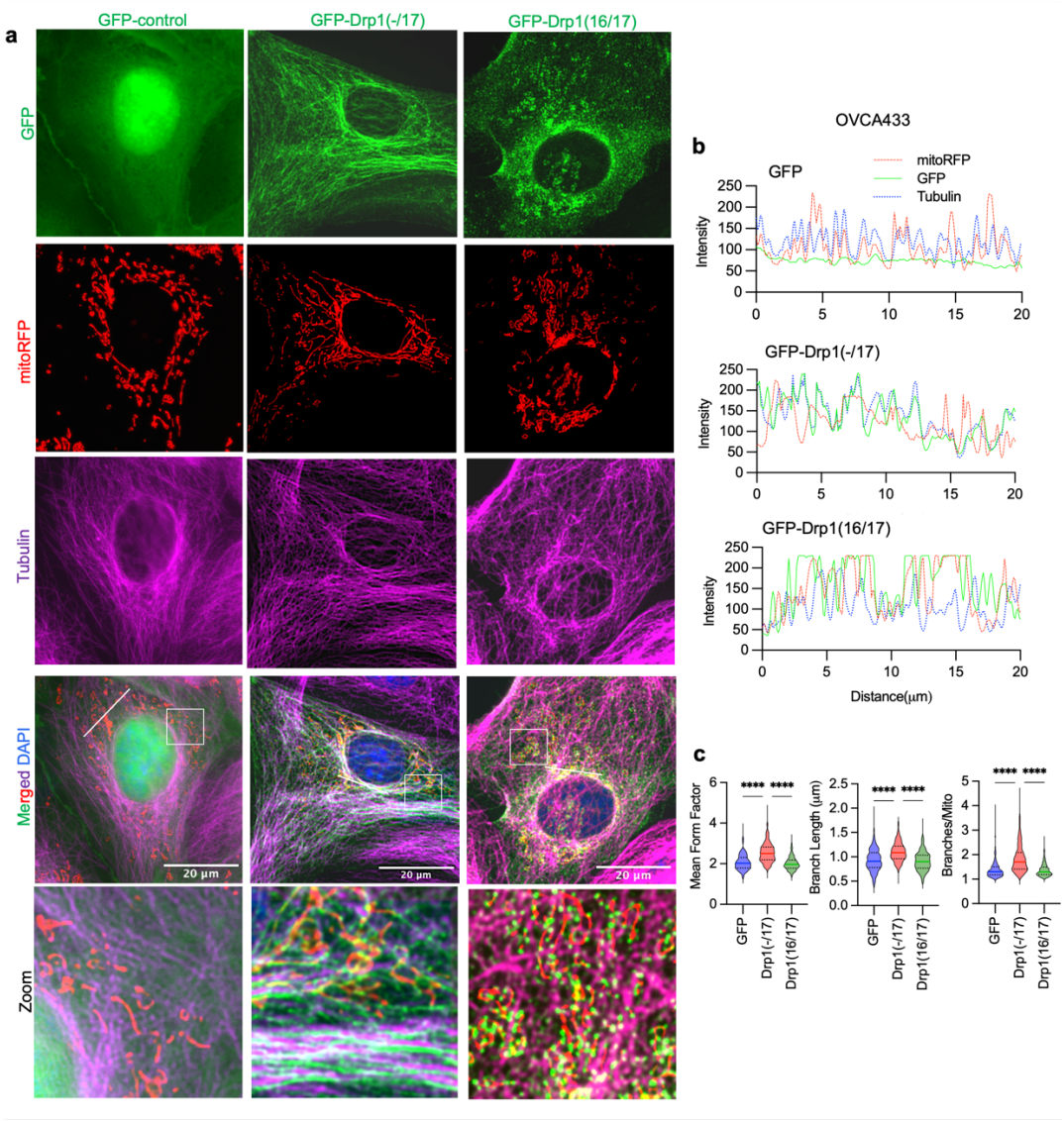


**Extended Data Figure 6. Drp1(-/17) displays decreased association with mitochondria in response to FCCP.**

a. Drp1(-/17) preserves its localization with Tubulin even upon treatment with the fission stimulus FCCP. In contrast, Drp1(16/17) cells have increased fission puncta staining at mitochondria in response to FCCP. Representative epifluorescence images of mitochondrial morphology and Drp1 distribution after 30 minutes with FCCP treatment (1μM) in OVCA433 cells. (Green: GFP or GFP-tagged Drp1, Red: mitochondria targeted RFP, Magenta: anti-Tubulin, Blue: DAPI; Scale bar: 20 μm).

b. Representative histogram of fluorescence intensity (white line in images on right) of GFP-Drp1 (green) in conjunction with mitochondria (red) and Tubulin (blue), illustrates that GFP-Drp1(16/17) strongly overlaps with mitochondria following FCCP treatment (1 μM, 30 mins). Conversely, Drp1(-/17) even with a pro-fission stimulus has higher overlapping peaks with tubulin than mitochondria, demonstrating decreased mitochondrial association.

c. Drp1(16/17) and GFP control cells show the anticipated reduction in mitochondrial size and increased fragmentation with FCCP, in contrast to Drp1(-/17) cells which continue to maintain elongated mitochondria. Quantification of mitochondrial morphological represented by three independent descriptors as analyzed by mitochondria analyzer in ImageJ. n = 301 cells from GFP-control, n = 285 cells from Drp1(-/17) and n=287 from Drp1(16/17) were analyzed. (one-way ANOVA Mean Form Factor $p < 0.0001$; Branch Length $p < 0.0001$ and Branches/mito $p<0.0001$. Tukey's post test *$p<0.05$, ****$p < 0.0001$).

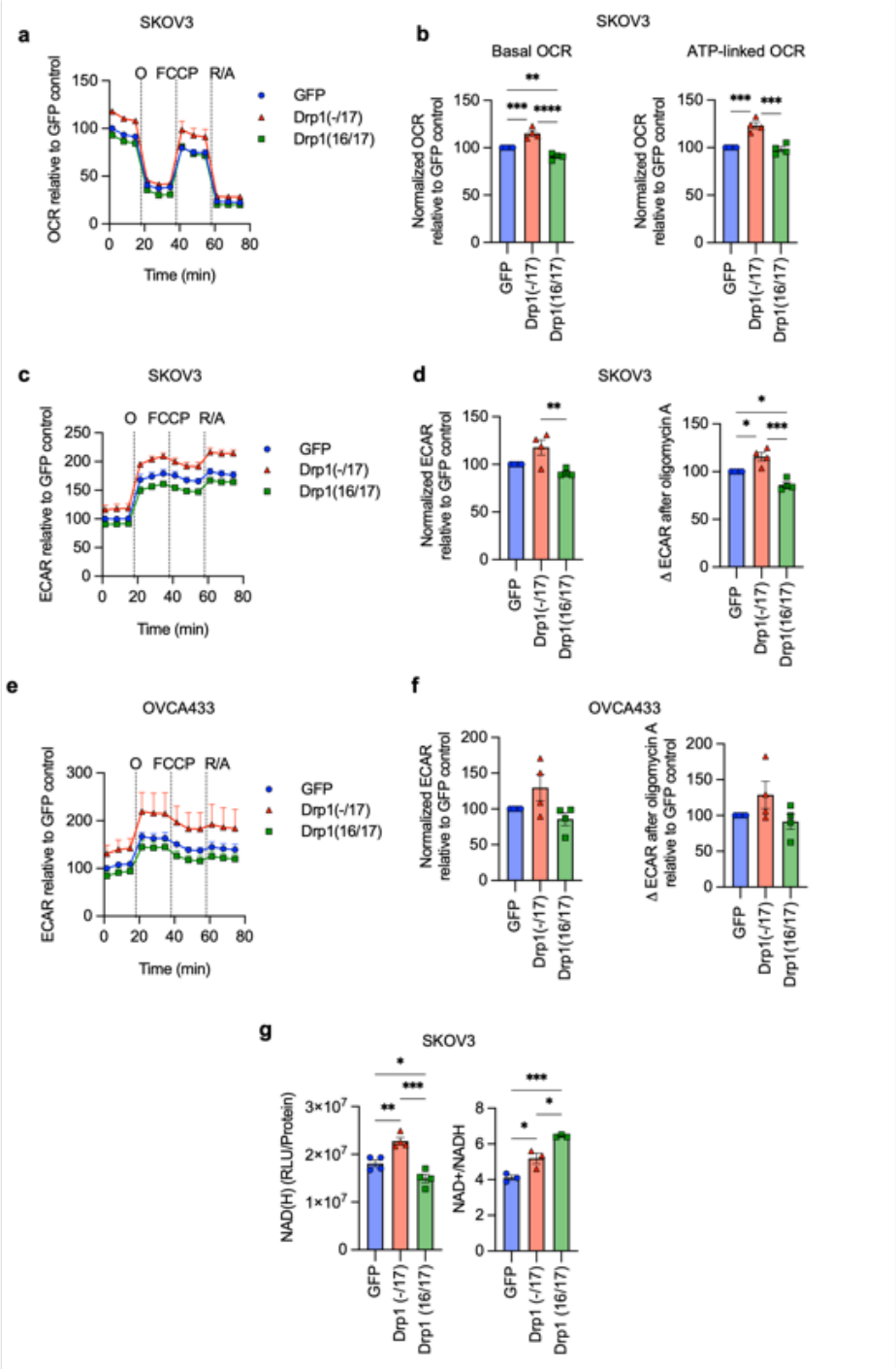


**Extended Data Figure 7. Expression of Drp1(-/17) splice variant increases mitochondrial respiration in SKOV3 cells.**

a. Expression of Drp1(-/17) increases oxygen consumption rates (OCR) in SKOV3 cells as assessed by mitochondrial stress test using Seahorse extracellular flux analysis (O: oligomycin A, R/A: rotenone/antimycin A; OCR is normalized to cell viability and expressed relative to GFP control, n=4)

b. Basal OCR and ATP-linked OCR are increased in cells expressing Drp1(-/17) compared to Drp1(16/17). Data are expressed relative to GFP control (n=4, one-way ANOVA Basal OCR $p<0.0001$; ATP-linked OCR $p=0.0001$; Tukey's post test $*p<0.05$, $**p<0.01$)

1441 c. Extracellular acidification rates (ECAR) of SKOV3 cells expressing GFP control, Drp1(-/17) or Drp1(16/17).
1442 ECAR traces are derived in parallel to OCR values from mitochondrial stress test.
1443 d. Basal ECAR and ΔECAR following oligomycin A inhibition of ATP-synthase were quantified in SKOV3 cells
1444 expressing GFP control, Drp1(-/17) or Drp1(16/17) (n=4, one-way ANOVA Basal ECAR p=0.0088; ΔECAR
1445 p=0.0003; Tukey's post test *p<0.05, **p<0.01, ***p<0.001).
1446 e. ECAR traces from OVCA433 cells expressing GFP control, Drp1(-/17) or Drp1(16/17).
1447 f. Basal ECAR and ΔECAR following oligomycin A inhibition of ATP-synthase were quantified in OVCA433
1448 cells expressing GFP control, Drp1(-/17) or Drp1(16/17) (n=4, one-way ANOVA Basal ECAR p=0.0743;
1449 ΔECAR p=0.1501).
1450 g. Total NAD(H) levels are increased in response to Drp1(-/17) expression relative to SKOV3 cells expressing
1451 GFP control or Drp1(16/17), while the ratio of NAD+/NADH is significantly decreased (one-way ANOVA
1452 NAD(H) n=4, p=0.0002; NAD+/NADH n=3 p=0.0004; Tukey's post test *p<0.05, ***p<0.001, ****p<0.0001).

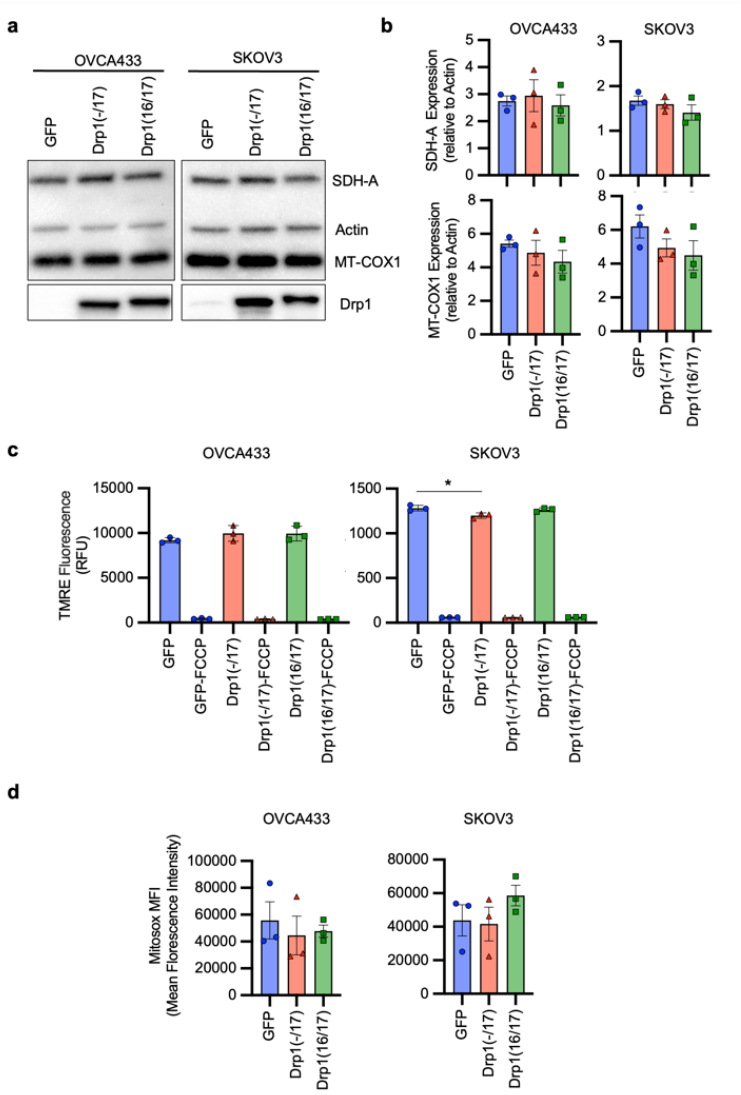


**Extended Data Figure 8. Expression of Drp1 (-/17) or Drp1(16/17) does not affect protein levels of ETC components or mitochondrial membrane potential in ovarian cancer cells.**

a. Levels of nuclear-DNA encoded SDH-A (Complex II) and mitochondrial-DNA encoded COX-1 (Complex IV) proteins are unchanged in both Drp1(-/17) and Drp1(16/17) expressing cells compared to GFP control cells. Data from one experimental replicate western blot is shown.
b. Quantification of SDH-A and MT-COX1 protein expression normalized to β-Actin in OVCA433 and SKOV3 cells by densitometry using ImageJ. (n=3, one-way ANOVA SDH-A expression; OVCA433 p=0.8407, SKOV3 p=0.3893, MT-COX1 expression; OVCA333 p=0. 4876, SKOV3 p=0. 2842).
c. Mitochondrial membrane potential was measured using TMRE (100nM) at baseline and with FCCP treatment (10 μM, 30 mins) in OVCA433 and SKOV3 cells expressing GFP control, Drp1(-/17) or Drp1(16/17) (n=3, one-way ANOVA of untreated cells OVCA433 p=0.3908, SKOV3 p=,0.0256, Tukey's post test *p=0.0264; one-way ANOVA comparison of FCCP treated cells OVCA433 p=0.3449, SKOV3 p=0.1715).
d. Drp1(-/17) and Drp1(16/17) overexpression in OVCA433 and SKOV3 cells did not alter MitoSox fluorescence, a mitochondrial targeted dye susceptible to superoxide mediated oxidation (n=3, one-way ANOVA OVCA433 p=0.7971, SKOV3=0.3830).

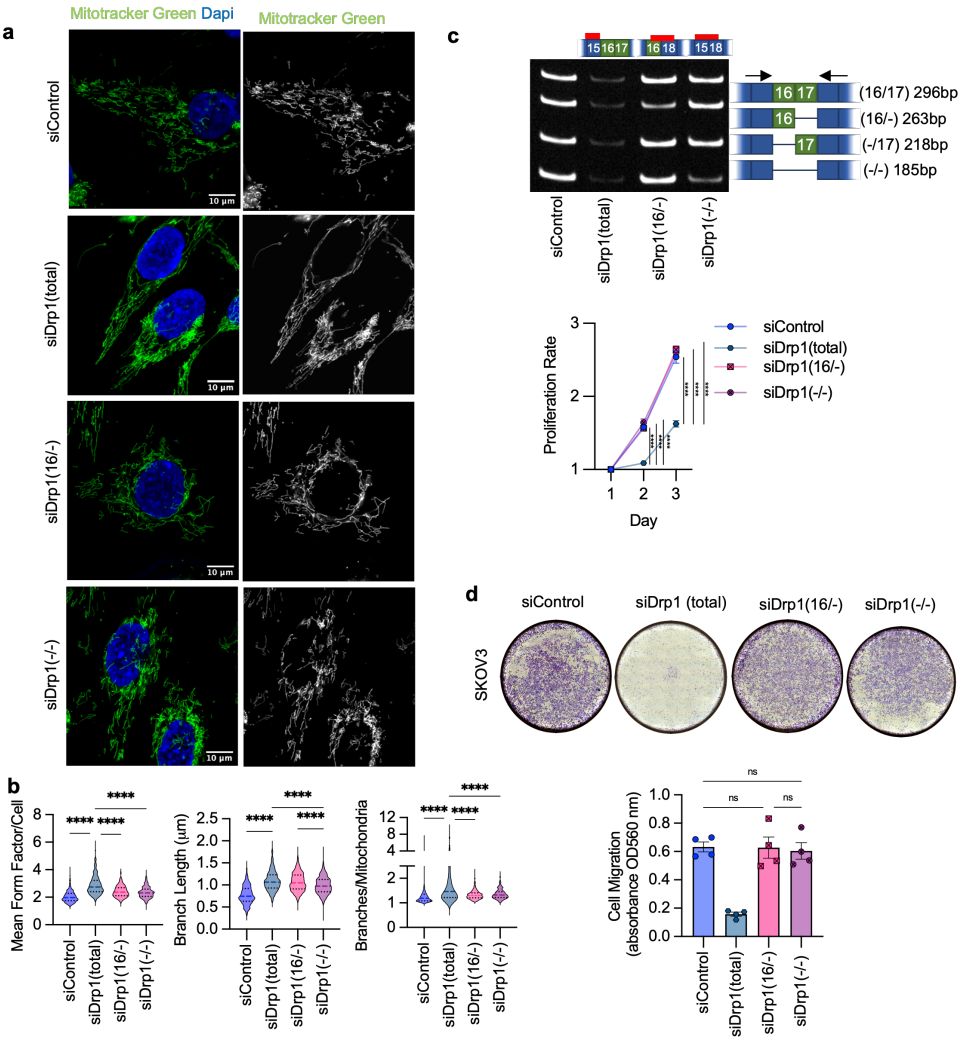


**Extended Data Figure 9. Specific knock-down of endogenous Drp1(-/-) and Drp1(16/-) variants and effects on mitochondrial morphology, cell proliferation and migration.**

a. Representative epifluorescence images of mitochondrial morphology upon splice variant specific siRNA Drp1 knockdown in SKOV3 cells. (Green: mitochondria stained with mitotracker green and Blue: DAPI). Scale bar: 10 µm.

b. Quantification of mitochondrial morphological represented by three independent descriptors as analyzed by mitochondria analyzer in ImageJ. (n = 560 cells from siControl, n = 334 cells from siDrp1(total), n=630 from siDrp1(16/17), n=655 from siDrp1(-/17) and n=555 from siDrp1(-/-)&(16/-) were analyzed. (one-way ANOVA Mean Form Factor p <0.0001; Branch Length p <0.0001 and Branches/mito p<0.0001. Tukey's post test was performed to assess differences between groups and analysis comparing groups to siDrp1(total) are shown, ****p <0.0001).

c. Drp1(-/-) and Drp1(16/-) variant specific knockdown did not alter cell proliferation in SKOV3 cells as no difference in proliferation rate compared to siControl cells. Cell proliferation was assessed by FluoReporter dsDNA quantification and proliferation rate expressed as increase in the cell density relative to day 1 (n=4, two-way ANOVA group factor variance p<0.0001, Tukey's post test ****p < 0.0001).

d. Cell migration was unchanged upon knock-down of Drp1(-/-) and Drp1(16/-) splice variants in SKOV3 cells. Post Drp1 knock-down, cell migration was assessed using the Boyden chamber transwell assay and quantified by measuring the absorbance of the crystal violet staining of migrated cells. Images are representative of 4 independent assays (n=4, one-way ANOVA ****p<0.0001. Tukey's post test was performed to assess differences between groups and analysis comparing siControl, siDrp1(16/17), siDrp1(-/17) and siDrp1(-/-)&(16/-) groups are shown).